



**QUEEN'S
UNIVERSITY
BELFAST**

Spectral Efficiency Analysis of Hybrid Relay-Reflecting Intelligent Surface-Assisted Cell-Free Massive MIMO Systems

Nguyen, N. T., Nguyen, V. D., Van Nguyen, H., Ngo, H. Q., Chatzinotas, S., & Juntti, M. (2022). Spectral Efficiency Analysis of Hybrid Relay-Reflecting Intelligent Surface-Assisted Cell-Free Massive MIMO Systems. *IEEE Transactions on Wireless Communications*, 1-20. Advance online publication. <https://doi.org/10.1109/TWC.2022.3217828>

Published in:

IEEE Transactions on Wireless Communications

Document Version:

Publisher's PDF, also known as Version of record

Queen's University Belfast - Research Portal:

[Link to publication record in Queen's University Belfast Research Portal](#)

Publisher rights

© 2022 The Authors.

This is an open access article published under a Creative Commons Attribution License (<https://creativecommons.org/licenses/by/4.0/>), which permits unrestricted use, distribution and reproduction in any medium, provided the author and source are cited.

General rights

Copyright for the publications made accessible via the Queen's University Belfast Research Portal is retained by the author(s) and / or other copyright owners and it is a condition of accessing these publications that users recognise and abide by the legal requirements associated with these rights.

Take down policy

The Research Portal is Queen's institutional repository that provides access to Queen's research output. Every effort has been made to ensure that content in the Research Portal does not infringe any person's rights, or applicable UK laws. If you discover content in the Research Portal that you believe breaches copyright or violates any law, please contact openaccess@qub.ac.uk.

Open Access

This research has been made openly available by Queen's academics and its Open Research team. We would love to hear how access to this research benefits you. – Share your feedback with us: <http://go.qub.ac.uk/oa-feedback>

Spectral Efficiency Analysis of Hybrid Relay-Reflecting Intelligent Surface-Assisted Cell-Free Massive MIMO Systems

Nhan Thanh Nguyen, *Member, IEEE*, Van-Dinh Nguyen, *Member, IEEE*, Hieu Van Nguyen, *Member, IEEE*, Hien Quoc Ngo, *Senior Member, IEEE*, Symeon Chatzinotas, *Senior Member, IEEE*, Markku Juntti, *Fellow, IEEE*

Abstract—A cell-free (CF) massive multiple-input-multiple-output (mMIMO) system can provide uniform spectral efficiency (SE) with simple signal processing. On the other hand, a recently introduced technology called hybrid relay-reflecting intelligent surface (HR-RIS) can customize the physical propagation environment by simultaneously reflecting and amplifying radio waves in preferred directions. Thus, it is natural that incorporating HR-RIS into CF mMIMO can be a symbiotic convergence of these two technologies for future wireless communications. This motivates us to consider an HR-RIS-aided CF mMIMO system to utilize their combined benefits. We first model the uplink/downlink channels and derive the minimum-mean-square-error estimate of the effective channels. We then present a comprehensive analysis of SE performance of the considered system. Specifically, we derive closed-form expressions for the uplink and downlink SE. The results reveal important observations on the performance gains achieved by HR-RISs compared to conventional systems. The presented analytical results are also valid for conventional CF mMIMO systems and those aided by passive reconfigurable intelligent surfaces. Such results play an important role in designing new transmission strategies and optimizing HR-RIS-aided CF mMIMO systems. Finally, we provide extensive numerical results to verify the analytical derivations and the effectiveness of the proposed system design under various settings.

Index Terms—Cell-free massive MIMO, hybrid relay-reflecting intelligent surface, reconfigurable intelligent surface, massive MIMO, spectral efficiency.

I. INTRODUCTION

To meet the demand for ultra reliable, ubiquitous coverage, high spectral efficiency (SE), and low-latency wireless

The work of N. T. Nguyen and M. Juntti was supported by Academy of Finland under 6Genesis Flagship (grant 318927), EERA Project (grant 332362), Infotech Program funded by University of Oulu Graduate School. The work of V.-D. Nguyen, H. V. Nguyen, and S. Chatzinotas was supported by the Luxembourg National Research Fund (FNR) - RISOTTI Project, ref. FNR/C20/IS/14773976/RISOTTI. The work of H. Q. Ngo was supported by the U.K. Research and Innovation Future Leaders Fellowships under Grant MR/S017666/1. This article was submitted in part to the IEEE International Conference on Communications (ICC), 2022.

N. T. Nguyen and M. Juntti are with Centre for Wireless Communications, University of Oulu, P.O.Box 4500, FI-90014, Finland, (email: nhan.nguyen@oulu.fi, markku.juntti@oulu.fi).

V.-D. Nguyen is with the College of Engineering and Computer Science, VinUniversity, Vinhomes Ocean Park, Hanoi 100000, Vietnam (e-mail: dinh.nv2@vinuni.edu.vn).

H. V. Nguyen is with the Faculty of Electronics and Telecommunication Engineering, The University of Danang — University of Science and Technology, Da Nang 50000, Vietnam (e-mail: nvhieu@dut.udn.vn).

S. Chatzinotas is with the Interdisciplinary Centre for Security, Reliability and Trust (SnT), University of Luxembourg, L-1855 Luxembourg, (email: symeon.chatzinotas@uni.lu).

H. Q. Ngo is with the School of Electronics, Electrical Engineering and Computer Science, Queen's University Belfast, Belfast BT7 1NN, United Kingdom (email: hien.ngo@qub.ac.uk).

communications, several new network architectures and technologies have been introduced recently. Among them, cell-free (CF) massive multiple-input-multiple-output (mMIMO) technology is a scalable version of MIMO networks, where a large number of access points (APs) are deployed in a large area to coherently serve numerous users in the same time-frequency resource [1]. CF mMIMO is capable of avoiding inter-cell interference and providing uniform quality-of-service (QoS) to all users in the network with simple signal processing techniques [2]. On the other hand, reconfigurable intelligent reflecting surface (RIS) is also considered as a promising technology towards sustainable wireless systems [3]. RISs can customize and program the physical propagation environment by reflecting radio waves in preferred directions with very low power consumption [4], [5]. As a result, RISs have been introduced as a cost- and energy-efficient solution to improve the performance of wireless communications systems [3]. A downside of passive RISs in a typical cellular network is the cascaded fading effect that will limit system performance. This inherent issue is effectively addressed by our proposed hybrid relay-reflecting intelligent surface (HR-RIS) [6]–[8]. In HR-RIS, only a few elements are active to amplify the incident signals, introducing relaying gains while maintaining the reflecting gains of conventional passive RISs, and in turn providing performance improvements in terms of SE and energy efficiency (EE). Therefore, HR-RIS-assisted CF mMIMO systems can be considered as a symbiotic convergence of these two technologies for future wireless communications.

A. Related Works

RISs have attracted great interest in the literature recently [9]–[14]. Their potential performance gains have been analyzed and optimized in various wireless communications systems, ranging from single/multiple-input-single-output (SISO/MISO) [15]–[22] to MIMO systems [23]–[27]. In particular, it has been shown that in a MISO system, the RIS of N passive elements can achieve a total beamforming gain of N^2 [16] and allow the received signal power to increase quadratically with N [17]. Furthermore, RISs can enrich the propagation channel of point-to-point MIMO systems by introducing additional propagation paths with different spatial angles, and thus, enhancing channel rank and multiplexing gain [28]. However, the beamforming design/optimization for RISs is generally challenging due to the non-convexity and large-sized variables (corresponding to the large number of RIS elements). In [23], an alternating optimization (AO)

method was developed to find an efficient solution for phase shifts. Perović *et al.* in [26] proposed the projected gradient method (PGM) to achieve the same achievable rate as that in the AO method, but with lower computational complexity and faster convergence. Another challenge in resource allocation of RISs is to acquire the channel state information (CSI) of reflected links. Most of the existing studies (e.g., [23], [26]) assumed the availability of perfect CSI, which is, however, much more difficult to acquire compared to the conventional systems without RISs [29], [30]. Concerning this challenge, the works [27] and [31] considered partial CSI, while efficient channel estimation schemes were proposed in [32]–[34]. The performances of communications systems assisted by practical RISs with limited phase shifts and hardware impairments were characterized in [21], [25], [35]–[37].

Unlike the aforementioned works, which often considered a single RIS to assist point-to-point communications systems, RIS-aided CF mMIMO systems were investigated in [38]–[41]. Specifically, Zhang *et al.* [38] proposed the deployment of numerous RISs to assist communications between a base station (BS) to user equipments (UEs). This work is then extended to a practical CF mMIMO system in [39], where multiple RISs are placed around multiple APs and users to enhance the EE performance. Zhang *et al.* [39] showed that deploying a small number of small-to-moderate-sized RISs provides an EE improvement, but when numerous and/or large-sized RISs are used, the EE performance is significantly degraded. In [40], Huang *et al.* proposed a fully decentralized design framework for cooperative beamforming in RIS-aided CF MIMO networks. Simulation results showed that the system sum-rate of CF networks significantly increases as aided by RISs and clearly outperforms the existing decentralized methods. Zhou *et al.* in [42] consider an achievable rate maximization for aerial RIS-aided CF mMIMO system, in which the transmit beamforming at APs and reflecting coefficients at the RIS are jointly optimized via AO. In [41], Trinh *et al.* further verified the benefits of deploying RISs in CF mMIMO systems where channel spatial correlation is taken into consideration.

It is worth noting that in the aforementioned RIS-aided cellular or CF (massive) MIMO systems, RISs only offer passive reflecting gains. Unless very large-sized RISs are employed, such gains are generally limited compared to those provided by conventional relays [16], [43]; however, the remarkable gains of relays come at the cost of high power consumption. HR-RIS introduced in [6]–[8] is capable of balancing this tradeoff. It can leverage the advantages of both passive RIS and active full-duplex (FD) amplify-and-forward (AF) relay to offer not only the reflecting but also relaying gains to the aided systems. In this regard, HR-RISs enable a semi-passive beamforming concept, ensuring a significant performance improvement in terms of SE and EE [6]–[8], [14], [44], [45]. Along with HR-RIS, a similar architecture named the *active RIS* has been recently proposed to exploit power amplifying gains [46]–[50]. The major difference between HR-RIS and active RIS is in the portion of active elements. More precisely, in the former, only a single or few RIS elements are activated by employing the low-power reflection amplifiers [51] or installing low-power RF chains and power amplifiers (PAs). In the latter,

on the other hand, all the elements are active. Although the performance gains offered by the HR-RIS and active RIS are investigated in different communications systems, i.e., MIMO systems in [6]–[8] and MISO systems in [46], all the works confirm that a few active elements are sufficient to ensure satisfactory improvement in SE, and excessive use of active elements can cause a significant loss in SE when the active power budget is limited. Furthermore, it has been shown in [6]–[8] that deploying numerous elements can severely degrade the EE performance. Therefore, it is reasonable to activate a small number of elements as in HR-RISs. Finally, we note that in the RIS architectures proposed in [33], [52], the active elements with RF chains denote active *receive*, not *transmit* processing. Thereby the active elements facilitate channel estimation, but do not amplify incident signals.

B. Contributions

This work, for the first time, considers a novel HR-RIS-aided CF mMIMO system where multiple HR-RISs are deployed to assist communications between APs and UEs. In the network, each HR-RIS serves as both active relay and passive reflecting surface to enable semi-passive beamforming, where only a few elements are required to be active. In what follows, we focus on characterizing the SE performance of the system and justifying the performance improvement offered by the deployed HR-RISs. Our main contributions are summarized as follows:

- We first model the uplink and downlink signal of the novel HR-RIS-aided CF mMIMO systems and derive the minimum-mean-square-error (MMSE) estimate of the effective channels in the time-division duplex (TDD) operation. This channel estimate is required for the conjugate beamforming in the downlink transmission and signal detection using matched filtering in the uplink. This result overcomes the limitations of most previous works which consider the ideal assumption of perfect CSI availability, which is unrealistic in practice.
- We provide rigorous closed-form expressions for the downlink and uplink SE of the considered system. Our analytical derivations are also valid for conventional CF mMIMO systems with and without purely passive RISs as they are special cases of the considered HR-RIS-aided CF mMIMO system. To the best of our knowledge, the analytical results on the SE performance of the passive RIS-aided CF mMIMO systems under the Rician fading channels have not been provided in the literature.
- From the SE closed-form expressions, we provide important insights into the power and SE gains introduced by HR-RISs. Specifically, we show that HR-RISs with the capability of amplifying the incident signals can overcome the (multiplicative) double path loss in the reflecting channels and enhance the SE of the UEs with poor channel conditions.
- The performance of the considered system is analyzed and justified through extensive simulation results under various deployment scenarios and setups. They also numerically demonstrate the SE performance improvement attained by implementing HR-RISs with respect

to the state-of-the-art approaches (e.g., conventional CF mMIMO and RIS-aided CF mMIMO systems).

The outcomes of this work also provide a novel framework and guidance for designing new transmission strategies and optimizing the performance of RIS/HR-RIS-enabled systems. In particular, the derived closed-form expressions of SE can be employed/leveraged as a design goal to maximize SE and EE. Furthermore, the developed system model and insights outlined in this paper facilitate further investigations and modifications of CF mMIMO systems with the presence of RISs/HR-RISs. Similar to [1], [2], we aim at deriving the closed-form SE based on the hardening bound. However, the difference is that in this work, the HR-RISs and Rician fading channels with spatially correlated non-line-of-sight (NLoS) components are taken into consideration. Thus, the signal model, analysis, and insights observed in those previous works are not applicable, and it is much more challenging to derive the MMSE channel estimate as well as the closed-form SE performance.

C. Paper Structure and Notation

The rest of the paper is organized as follows. In Section II, we present mathematical models of HR-RIS and the uplink channel as well as MMSE estimation of the effective uplink channels. Then, the signal models of the downlink and uplink data transmission are presented in Section III. We derive closed-form expressions for downlink and uplink SE in Section IV. Numerical results are given in Section V, while Section VI concludes the paper.

Notations: Throughout the paper, numbers, vectors, and matrices are denoted by lower-case, bold-face lower-case, and bold-face upper-case letters, respectively. We denote by $(\cdot)^*$, $(\cdot)^T$, and $(\cdot)^H$ the conjugate of a complex number, the transpose and conjugate transpose of a matrix or vector, respectively. Whereas, $\text{diag}\{a_1, \dots, a_N\}$ represents a diagonal matrix with diagonal entries a_1, \dots, a_N . Furthermore, $|\cdot|$ denotes either the absolute value of a scalar or cardinality of a set. $\mathbb{E}\{\cdot\}$ and $\text{Var}\{\cdot\}$ are the expected value and variance of a random variable, respectively, while $\mathbb{C}\{\cdot\}$ and $\mathbb{C}\{\cdot, \cdot\}$ denote the auto- and cross-covariance operators, respectively. Finally, \circ represents a Hadamard product.

II. HR-RIS, CHANNEL MODEL AND ESTIMATION

We consider an HR-RIS-aided CF mMIMO system illustrated in Fig. 1(a), where L APs, each equipped with N_A transmit antennas, simultaneously serve K single-antenna UEs. Furthermore, the system is aided by M HR-RISs. The following further assumptions are made. First, all APs are connected to the CPU via ideal backhaul links that offer error-free and infinite capacity [1]. Second, we assume the TDD operation, where each coherence interval is divided into three main phases, including uplink training, uplink payload data transmission, and downlink payload data transmission. Furthermore, the deployment of HR-RISs/RISs is assumed to preserve the channel reciprocity as in [32], [53], [54]. Therefore, the uplink and downlink channel coefficients are the same, and, thus, we rely on uplink channel estimation

for both downlink and uplink transmission. In practice, some calibration schemes may be needed, but those are out of the scope of this paper. To model the HR-RIS-aided CF mMIMO system, we first present a mathematical model of HR-RIS. The details on its architecture can be found in [7], [8].

A. Deployment of HR-RISs

Each HR-RIS is equipped with N elements, including N_R active relay elements and $N - N_R$ passive reflecting elements. Here we note that an active elements would generally require higher power consumption and hardware cost than a passive one [46]. Furthermore, deploying numerous active elements can severely degrade the system performance in terms of EE and SE when the HR-RIS's power budget is limited [7], [8]. Therefore, it is reasonable to deploy the HR-RIS with a few active elements (i.e., $N_R \ll N$), which is sufficient to provide good SE improvement and maintain a low hardware cost [7]. Denote by $\mathcal{A}_m \subset \{1, 2, \dots, N\}$ with $|\mathcal{A}_m| = N_R$ the index set of the active elements in the m -th HR-RIS, which is assumed to be fixed and given in advance (during the manufacturing of HR-RISs). The amplitude of passive reflecting coefficients is fixed to unity, which is optimal in the sense that it maximizes the received signal power [16], and their phases are tunable in the range $[0, 2\pi)$. In contrast, both the phase and amplitude of active relaying coefficients can be optimized for efficient relaying. Let α_{mn} be the relay/reflection coefficient of the n -th element in the m -th HR-RIS. In other words, we have $\alpha_{mn} = |\alpha_{mn}|e^{j\theta_{mn}}$, where $\theta_{mn} \in [0, 2\pi)$ represents the phase shift, and $|\alpha_{mn}| = 1$ for $n \notin \mathcal{A}_m$. Let $\Upsilon_m = \text{diag}\{\alpha_{m1}, \dots, \alpha_{mN}\} \in \mathbb{C}^{N \times N}$ be the diagonal matrix of the coefficients of the m -th HR-RIS. We define an additive decomposition as $\Upsilon_m = \Psi_m + \Phi_m$. Here, $\Psi_m = \mathbb{1}_m \circ \Upsilon_m$ and $\Phi_m = (\mathbf{I}_N - \mathbb{1}_m) \circ \Upsilon_m$, where $\mathbb{1}_m$ denotes an $N \times N$ diagonal matrix whose non-zero diagonal elements are all unity and have positions determined by \mathcal{A}_m . In particular, Ψ_m and Φ_m contain only active relaying and passive reflecting coefficients of the m -th HR-RIS, respectively. Clearly, HR-RIS reduces to a standard passive RIS if $|\alpha_{mn}| = 1, \forall m, n$.

The simultaneous reflecting and amplifying at active elements can be realized by the recently introduced technology called *reflection amplifiers* [51]. We note that in an active element, the incident signal is only amplified without decoding. Therefore, the delay when the signals go through active elements is much smaller than the coherence interval and has no impact on the channel estimation and signal combining at the receiver as in [33], [46]–[50]. Similarly, the reflection amplifier-based AF relay does not cause significant self-interference levels, but we still include it in our analysis for completeness.

B. Channel Model

As illustrated in Fig. 1(c), when a UE sends its pilot sequence to the l -th AP, the pilot signal propagates through both the direct UE-AP channel and M HR-RISs. Accordingly, we denote $\mathbf{h}_{lk}^{\text{UA}} \in \mathbb{C}^{N_A \times 1}$, $\mathbf{h}_{km}^{\text{US}} \in \mathbb{C}^{N \times 1}$, and $\mathbf{H}_{lm}^{\text{SA}} \in \mathbb{C}^{N_A \times N}$ as the channels between the k -th UE and the l -th AP, between

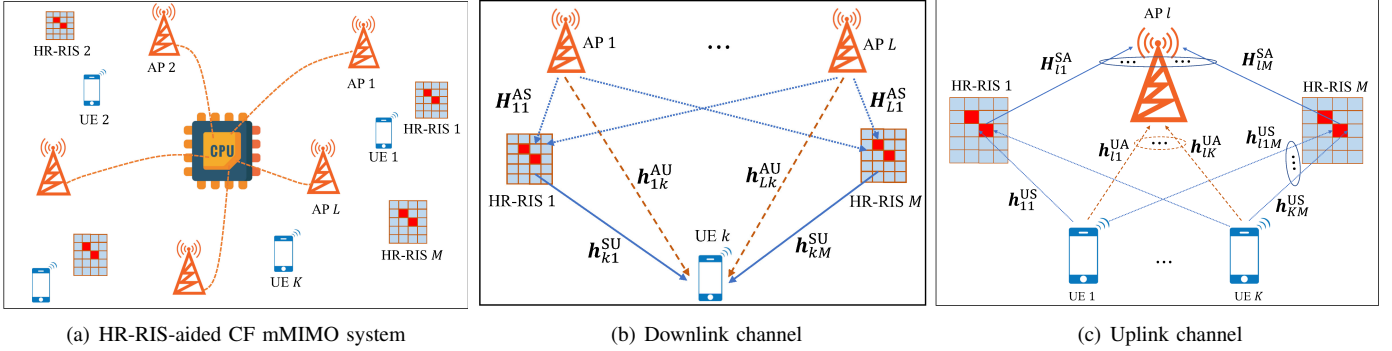


Fig. 1. The HR-RIS-aided CF mMIMO system and its downlink and uplink channels.

the k -th UE and the m -th HR-RIS, and between the m -th HR-RIS and the l -th AP, respectively.

In practice, wireless channels typically consist of a deterministic LoS path and non-deterministic component caused by multi-path propagation [55]. Therefore, we consider the Rician fading model for the channels $\mathbf{h}_{lk}^{\text{UA}}$, $\mathbf{h}_{km}^{\text{US}}$, and $\mathbf{H}_{lm}^{\text{SA}}$ [16], [23], with the Rician factors κ_{lk}^{UA} , κ_{km}^{US} , and κ_{lm}^{SA} , respectively. Furthermore, we assume the slow mobility of the users and small phase noise, and thus, the LoS components in $\bar{\mathbf{h}}_{lk}^{\text{UA}}$ and $\bar{\mathbf{h}}_{km}^{\text{US}}$ are deterministic.¹ In particular, $\mathbf{h}_{lk}^{\text{UA}}$ is modeled as

$$\mathbf{h}_{lk}^{\text{UA}} = \sqrt{\zeta_{lk}^{\text{UA}}} \left(\sqrt{\frac{\kappa_{lk}^{\text{UA}}}{\kappa_{lk}^{\text{UA}} + 1}} \bar{\mathbf{h}}_{lk}^{\text{UA}} + \sqrt{\frac{1}{\kappa_{lk}^{\text{UA}} + 1}} \tilde{\mathbf{h}}_{lk}^{\text{UA}} \right), \quad (1)$$

where ζ_{lk}^{UA} denotes the large-scale fading; $\bar{\mathbf{h}}_{lk}^{\text{UA}}$ and $\tilde{\mathbf{h}}_{lk}^{\text{UA}}$ represent the line-of-sight (LoS) and NLoS components, respectively. The former is modeled as a deterministic channel with known amplitude, while the latter is assumed to follow the Rayleigh fading model [16], [23]. Therefore, we have $|\bar{h}_{lkt}^{\text{UA}}| = 1$, where $\bar{h}_{lkt}^{\text{UA}}$ denote the t -th element of $\bar{\mathbf{h}}_{lk}^{\text{UA}}$, $t = 1, \dots, N_A$. We consider the spatial correlation among the antennas at each AP, but we assume that the HR-RISs have sufficiently large physical size so that the correlation among their elements are negligible. Let $\mathbf{Q}_{lk}^{\text{A}} \in \mathbb{C}^{N_A \times N_A}$ with $\text{trace}(\mathbf{Q}_{lk}^{\text{A}})/N_A = 1$ be the correlation matrix at the l -th AP, associated with the NLoS channel $\tilde{\mathbf{h}}_{lk}^{\text{UA}}$. Then, we have $\tilde{\mathbf{h}}_{lk}^{\text{UA}} \sim \mathcal{CN}(\mathbf{0}, \mathbf{Q}_{lk}^{\text{A}})$. It is observed from (1) that element h_{lkt}^{UA} of $\mathbf{h}_{lk}^{\text{UA}}$ has mean value

$$\mu_{lkt}^{\text{UA}} \triangleq \sqrt{\zeta_{lk}^{\text{UA}}} \sqrt{\frac{\kappa_{lk}^{\text{UA}}}{\kappa_{lk}^{\text{UA}} + 1}} \bar{h}_{lkt}^{\text{UA}}, \quad t = 1, \dots, N_A. \quad (2)$$

By defining $\boldsymbol{\mu}_{lk}^{\text{UA}} \triangleq [\mu_{lk1}^{\text{UA}}, \dots, \mu_{lkN_A}^{\text{UA}}]^T$ as the mean vector of $\mathbf{h}_{lk}^{\text{UA}}$, and by denoting $\beta_{lk}^{\text{UA}} \triangleq \frac{\zeta_{lk}^{\text{UA}}}{\kappa_{lk}^{\text{UA}} + 1}$, we rewrite (1) as

$$\mathbf{h}_{lk}^{\text{UA}} = \boldsymbol{\mu}_{lk}^{\text{UA}} + \sqrt{\beta_{lk}^{\text{UA}}} \tilde{\mathbf{h}}_{lk}^{\text{UA}}. \quad (3)$$

Similarly, let $\{\zeta_{km}^{\text{US}}, \zeta_{lm}^{\text{SA}}\}$, $\{\bar{h}_{kmn}^{\text{US}}, \bar{h}_{lmt}^{\text{SA}}\}$, and $\{\tilde{h}_{kmn}^{\text{US}}, \tilde{h}_{lmt}^{\text{SA}}\}$ for $n = 1, \dots, N$, $t = 1, \dots, N_A$ be the large-scale fading, LoS, and NLoS components of the elements of $\mathbf{h}_{km}^{\text{US}}$ and $\mathbf{H}_{lm}^{\text{SA}}$,

respectively. Similar to (3), let us denote

$$\mu_{kmn}^{\text{US}} \triangleq \sqrt{\zeta_{km}^{\text{US}}} \sqrt{\frac{\kappa_{km}^{\text{US}}}{\kappa_{km}^{\text{US}} + 1}} \bar{h}_{kmn}^{\text{US}}, \quad n = 1, \dots, N, \quad (4)$$

$$\mu_{lmt}^{\text{SA}} \triangleq \sqrt{\zeta_{lm}^{\text{SA}}} \sqrt{\frac{\kappa_{lm}^{\text{SA}}}{\kappa_{lm}^{\text{SA}} + 1}} \bar{h}_{lmt}^{\text{SA}}, \quad t = 1, \dots, N_A, \quad (5)$$

$\beta_{km}^{\text{US}} \triangleq \frac{\zeta_{km}^{\text{US}}}{\kappa_{km}^{\text{US}} + 1}$, and $\beta_{lm}^{\text{SA}} \triangleq \frac{\zeta_{lm}^{\text{SA}}}{\kappa_{lm}^{\text{SA}} + 1}$. Here, μ_{kmn}^{US} and μ_{lmt}^{SA} are the mean value/vector of h_{kmn}^{US} and h_{lmt}^{SA} , respectively, where h_{kmn}^{US} is the n -th element of $\mathbf{h}_{km}^{\text{US}}$, and h_{lmt}^{SA} is the n -th column of $\mathbf{H}_{lm}^{\text{SA}}$. As a result, h_{kmn}^{US} and h_{lmt}^{SA} are modeled as

$$h_{kmn}^{\text{US}} = \mu_{kmn}^{\text{US}} + \sqrt{\beta_{km}^{\text{US}}} \tilde{h}_{kmn}^{\text{US}}, \quad (6)$$

$$\mathbf{h}_{lmt}^{\text{SA}} = \boldsymbol{\mu}_{lmt}^{\text{SA}} + \sqrt{\beta_{lm}^{\text{SA}}} \tilde{\mathbf{h}}_{lmt}^{\text{SA}}, \quad (7)$$

respectively. Here, we note that the NLoS channel $\tilde{\mathbf{h}}_{lmt}^{\text{SA}}$ is spatially correlated, i.e., $\tilde{\mathbf{h}}_{lmt}^{\text{SA}} \sim \mathcal{CN}(\mathbf{0}, \mathbf{Q}_{lmt}^{\text{A}})$, where $\mathbf{Q}_{lmt}^{\text{A}}$ represents the spatial correlation matrix with $\text{trace}(\mathbf{Q}_{lmt}^{\text{A}})/N_A = 1, \forall l, m, n$. The effective channel between the k -th UE and the l -th AP, denoted by $\mathbf{g}_{lk} \in \mathbb{C}^{N_A \times 1}$, can be expressed as

$$\begin{aligned} \mathbf{g}_{lk} &\triangleq \mathbf{h}_{lk}^{\text{UA}} + \sum_{m=1}^M \mathbf{H}_{lm}^{\text{SA}} \boldsymbol{\Upsilon}_m \mathbf{h}_{km}^{\text{US}} \\ &= \mathbf{h}_{lk}^{\text{UA}} + \sum_{m=1}^M \sum_{n=1}^N \alpha_{mnn} \mathbf{h}_{lmt}^{\text{SA}} h_{kmn}^{\text{US}}, \end{aligned} \quad (8)$$

where the last equality follows by the diagonal structure of $\boldsymbol{\Upsilon}_m$.

C. Uplink Channel Estimation

We first consider the uplink training phase, in which all UEs transmit their pilot sequences to the APs to perform channel estimation. Let $\sqrt{\tau_p} \boldsymbol{\varphi}_k \in \mathbb{C}^{\tau_p \times 1}$ be the pilot sequence of the k -th UE, where $\|\boldsymbol{\varphi}_k\|^2 = 1, \forall k$. Here, τ_p ($\tau_p < \tau_c$) is the length of $\boldsymbol{\varphi}_k$, where τ_c denotes the length of each coherence interval (in samples). The received pilot signal at the l -th AP is

$$\mathbf{Y}_l = \mathbf{Y}_l^{\text{UA}} + \mathbf{Y}_l^{\text{USA}} + \mathbf{Z}_{A,l}, \quad (9)$$

¹We refer readers to [56], [57] for possible extensions taking instantaneous phase shifts of LoS components into consideration.

where \mathbf{Y}_l^{UA} and $\mathbf{Y}_l^{\text{USA}}$ represent the received signals propagating through the direct UE-AP channel and those reflected through HR-RISs, respectively. In (9), $\mathbf{Z}_{A,l} \in \mathbb{C}^{N_A \times \tau_p}$ is a matrix of complex additive white Gaussian noise (AWGN) at the l -th AP, whose entries are $\mathcal{CN}(0, \sigma_A^2)$ random variables. Denoting by ρ_p the power of each UE to transmit the pilot signal, we have

$$\mathbf{Y}_l^{\text{UA}} = \sqrt{\tau_p \rho_p} \sum_{k=1}^K \mathbf{h}_{lk}^{\text{UA}} \varphi_k^H, \quad (10)$$

$$\begin{aligned} \mathbf{Y}_l^{\text{USA}} = & \sqrt{\tau_p \rho_p} \sum_{m=1}^M \sum_{k=1}^K \mathbf{H}_{lm}^{\text{SA}} \underbrace{\Upsilon_m \mathbf{h}_{km}^{\text{US}} \varphi_k^H}_{\text{amplified/reflected pilot signal}} \\ & + \sum_{m=1}^M \mathbf{H}_{lm}^{\text{SA}} \left(\underbrace{\Psi_m \mathbf{Z}_{\text{SI},m}}_{\text{amplified SI}} + \underbrace{\Psi_m \mathbf{Z}_{\text{N},m}}_{\text{amplified noise}} \right). \end{aligned} \quad (11)$$

It is shown in (11) that the l -th AP receives not only pilot signals but also self-interference (SI) $\mathbf{Z}_{\text{SI},m} \in \mathbb{C}^{N \times \tau_p}$ and noise $\mathbf{Z}_{\text{N},m} \in \mathbb{C}^{N \times \tau_p}$ from HR-RISs caused by active relay elements in $\mathcal{A}_m, \forall m$. We adopt the SI model in [58], in which the SI is modeled as $\mathcal{CN}(0, \sigma_{\text{SI}}^2)$ random variables. This is based on the fact that there are numerous sources of imperfections in active elements, and the experiment in [59] shows that the residual SI can be eliminated to be as low as 1 dB independent of the transmit power and the number of transmit antennas. We denote by $\mathbf{z}_{\text{SI},mn}^H$ and $\mathbf{z}_{\text{N},mn}^H$ the n -th row of $\mathbf{Z}_{\text{SI},m}$ and $\mathbf{Z}_{\text{N},m}$, respectively. Their elements are distributed as $\mathcal{CN}(0, \sigma_{\text{SI}}^2)$ and $\mathcal{CN}(0, \sigma_{\text{N}}^2)$, respectively, for $n \in \mathcal{A}_m$; otherwise, they are zeros because the n -th element ($n \notin \mathcal{A}_m$) of the m -th HR-RIS only reflects the incident pilot signals passively [60].

From (8)–(11), \mathbf{Y}_l can be written as

$$\mathbf{Y}_l = \sqrt{\tau_p \rho_p} \sum_{k=1}^K \mathbf{g}_{lk} \varphi_k^H + \mathbf{Z}_l, \quad (12)$$

where

$$\begin{aligned} \mathbf{Z}_l & \triangleq \mathbf{Z}_{A,l} + \sum_{m=1}^M \mathbf{H}_{lm}^{\text{SA}} \Psi_m (\mathbf{Z}_{\text{SI},m} + \mathbf{Z}_{\text{N},m}) \\ & = \mathbf{Z}_{A,l} + \sum_{m=1}^M \sum_{n=1}^N \alpha_{mn} \mathbf{h}_{lmn}^{\text{SA}} (\mathbf{z}_{\text{SI},mn} + \mathbf{z}_{\text{N},mn})^H, \end{aligned} \quad (13)$$

is the aggregated noise matrix at the l -th AP. Note that $\{\mathbf{Z}_{\text{SI},m}, \mathbf{Z}_{\text{N},m}, \mathbf{Z}_{A,l}, \mathbf{H}_{lm}^{\text{SA}}\}$ are mutually independent, and we recall from the definition of Ψ_m in Section II-A that in this matrix, only the diagonal entries with positions determined by \mathcal{A}_m are non-zeros. Thus, the entries of \mathbf{Z}_l have zero-mean and variance $\sigma_{p,l}^2$, given as

$$\sigma_{p,l}^2 = \sigma_A^2 + \sum_{m=1}^M \beta_{lm}^{\text{SA}} \sum_{n \in \mathcal{A}_m} |\alpha_{mn}|^2 \underbrace{(\sigma_{\text{N}}^2 + \sigma_{\text{SI}}^2)}_{\triangleq \sigma_{\text{Z}}^2}. \quad (14)$$

To estimate \mathbf{g}_{lk} , \mathbf{Y}_l is projected onto φ_k , yielding

$$\mathbf{y}_{lk} \triangleq \mathbf{Y}_l \varphi_k = \sqrt{\tau_p \rho_p} \mathbf{g}_{lk} + \sqrt{\tau_p \rho_p} \sum_{k' \neq k} \mathbf{g}_{lk'} \varphi_{k'}^H \varphi_k \tilde{\mathbf{z}}_{lk}, \quad (15)$$

where

$$\begin{aligned} \tilde{\mathbf{z}}_{lk} & = \mathbf{Z}_l \varphi_k \\ & = \left(\mathbf{Z}_{A,l} + \sum_{m=1}^M \sum_{n=1}^N \alpha_{mn} \mathbf{h}_{lmn}^{\text{SA}} (\mathbf{z}_{\text{SI},mn} + \mathbf{z}_{\text{N},mn})^H \right) \varphi_k. \end{aligned} \quad (16)$$

From (15), we derive the MMSE estimate of the effective channel \mathbf{g}_{lk} detailed in the following theorem.

Theorem 1: The MMSE estimate of \mathbf{g}_{lk} is given by

$$\hat{\mathbf{g}}_{lk} = \boldsymbol{\mu}_{lk} - \tau_p \rho_p \check{\mathbf{C}}_{lk} \mathbf{E}_{lk}^{-1} \check{\boldsymbol{\mu}}_{lk} + \sqrt{\tau_p \rho_p} \check{\mathbf{C}}_{lk} \mathbf{E}_{lk}^{-1} \mathbf{y}_{lk}, \quad (17)$$

where

$$\begin{aligned} \check{\boldsymbol{\mu}}_{lk} & \triangleq \sum_{k'=1}^K \varphi_{k'}^H \varphi_k \boldsymbol{\mu}_{lk'}, \\ \check{\mathbf{C}}_{lk} & \triangleq \mathbf{C}_{lk} + \sum_{k' \neq k} \varphi_{k'}^H \varphi_k \mathbf{C}_{lkk'}, \\ \mathbf{E}_{lk} & \triangleq \tau_p \rho_p \sum_{k'=1}^K |\varphi_{k'}^H \varphi_k|^2 \mathbf{C}_{lk'} + \sigma_{p,l}^2 \mathbf{I}_{N_A}. \end{aligned} \quad (18)$$

Here, $\boldsymbol{\mu}_{lk}$, \mathbf{C}_{lk} , and $\mathbf{C}_{lkk'}$ are the mean vector, covariance matrix of \mathbf{g}_{lk} , and the cross-covariance matrix between \mathbf{g}_{lk} and $\mathbf{g}_{lk'}$, given as

$$\boldsymbol{\mu}_{lk} = \boldsymbol{\mu}_{lk}^{\text{UA}} + \sum_{m=1}^M \sum_{n=1}^N \alpha_{mn} \boldsymbol{\mu}_{lmn}^{\text{SA}} \boldsymbol{\mu}_{kmn}^{\text{US}}, \quad (19)$$

$$\begin{aligned} \mathbf{C}_{lk} & = \beta_{lk}^{\text{UA}} \mathbf{Q}_{lk}^{\text{A}} \\ & + \sum_{m=1}^M \sum_{n=1}^N |\alpha_{mn}|^2 \left(\beta_{km}^{\text{US}} + |\mu_{kmn}^{\text{US}}|^2 \right) \beta_{lm}^{\text{SA}} \mathbf{Q}_{lmn}^{\text{A}} \\ & + \beta_{km}^{\text{US}} \boldsymbol{\mu}_{lmn}^{\text{SA}} (\boldsymbol{\mu}_{lmn}^{\text{SA}})^H, \end{aligned} \quad (20)$$

$$\mathbf{C}_{lkk'} = \sum_{m=1}^M \sum_{n=1}^N |\alpha_{mn}|^2 \mu_{kmn}^{\text{US}} (\mu_{k'mn}^{\text{US}})^* \beta_{lm}^{\text{SA}} \mathbf{Q}_{lmn}^{\text{A}}. \quad (21)$$

respectively. The estimate $\hat{\mathbf{g}}_{lk}$ has mean vector $\mathbb{E}\{\hat{\mathbf{g}}_{lk}\} = \boldsymbol{\mu}_{lk}$ and covariance matrix $\hat{\mathbf{C}}_{lk} = \tau_p \rho_p \check{\mathbf{C}}_{lk} \mathbf{E}_{lk}^{-H} \check{\mathbf{C}}_{lk}^H$, which yield

$$\begin{aligned} \mathbb{E}\{\hat{\mathbf{g}}_{lk} \hat{\mathbf{g}}_{lk}^H\} & = \hat{\mathbf{C}}_{lk} + \boldsymbol{\mu}_{lk} \boldsymbol{\mu}_{lk}^H \triangleq \hat{\mathbf{R}}_{lk}, \\ \mathbb{E}\{\|\hat{\mathbf{g}}_{lk}\|^2\} & = \text{trace}(\hat{\mathbf{C}}_{lk}) + \|\boldsymbol{\mu}_{lk}\|^2. \end{aligned} \quad (22)$$

The estimation error $\tilde{\mathbf{g}}_{lk} \triangleq \mathbf{g}_{lk} - \hat{\mathbf{g}}_{lk}$ is uncorrelated with $\hat{\mathbf{g}}_{lk}$ and has mean vector $\mathbb{E}\{\tilde{\mathbf{g}}_{lk}\} = \mathbf{0}$ and covariance matrix

$$\mathbb{C}\{\tilde{\mathbf{g}}_{lk}\} = \mathbf{C}_{lk} - \hat{\mathbf{C}}_{lk} \triangleq \tilde{\mathbf{R}}_{lk}. \quad (23)$$

Proof: Please see Appendix A. \square

It is observed from (17)–(21) that with given pilot sequences, each AP performs the MMSE estimation using only the received pilot signals and large-scale parameters of the direct and reflecting channels. Here, large-scale parameters are obtained under the assumption that the information on the path loss, Rician factors, deterministic LoS components, and correlation matrices are available [57], [61]. These parameters change much more slowly than small-scale fading channels (i.e. they stay constant for many coherence intervals of small-

scale fading), making the MMSE estimation practical in real systems [1].

III. DOWNLINK AND UPLINK SIGNAL MODEL

A. Downlink Payload Transmission

Let s_k be the symbol intended for the k -th UE, where $\mathbb{E}\{|s_k|^2\} = 1$, $k = 1, \dots, K$. Let $\mathbf{x}_l \in \mathbb{C}^{N_A \times 1}$ be the signal vector transmitted from the l -th AP to all the UEs. For simplicity, conjugate beamforming is adopted at APs [2], and each symbol s_k at the l -th AP is scaled by the power control coefficient η_{lk} and precoded with the conjugate of the channel estimate:

$$\mathbf{x}_l = \sqrt{\rho_d} \sum_{k=1}^K \sqrt{\eta_{lk}} \hat{\mathbf{g}}_{lk}^* s_k, \quad (24)$$

where ρ_d is the maximum transmit power at each AP.

Similar to the uplink, the downlink signals propagate on the direct channels and also reflects through HR-RISs, as illustrated in Fig. 1(b). For the ease of notation and due to the channel reciprocity, we denote the downlink channels as $\mathbf{h}_{lk}^{\text{AU}} = (\mathbf{h}_{lk}^{\text{UA}})^T \in \mathbb{C}^{1 \times N_A}$, $\mathbf{h}_{km}^{\text{SU}} = (\mathbf{h}_{km}^{\text{US}})^T \in \mathbb{C}^{1 \times N}$, and $\mathbf{H}_{lm}^{\text{AS}} = (\mathbf{H}_{lm}^{\text{SA}})^T \in \mathbb{C}^{N \times N_A}$. Similar to (9), the received signal at the k -th UE in the downlink can be expressed as

$$r_{d,k} = \sum_{l=1}^L \underbrace{\left(\mathbf{h}_{lk}^{\text{AU}} + \sum_{m=1}^M \mathbf{h}_{km}^{\text{SU}} \Upsilon_m \mathbf{H}_{lm}^{\text{AS}} \right)}_{\triangleq \mathbf{g}_{lk}^T} \mathbf{x}_l + \underbrace{\sum_{m=1}^M \mathbf{h}_{km}^{\text{SU}} \Psi_m (\mathbf{z}_{N,m} + \mathbf{z}_{\text{SI},m})}_{\triangleq z_{d,k}} + z_{U,k}, \quad (25)$$

where $z_{U,k} \sim \mathcal{CN}(0, \sigma_U^2)$ is the AWGN, $\mathbf{z}_{\text{SI},m} \sim \mathcal{CN}(\mathbf{0}, \sigma_{\text{SI}}^2 \mathbf{1}_m)$ is the residual SI, and $\mathbf{z}_{N,m} \sim \mathcal{CN}(\mathbf{0}, \sigma_N^2 \mathbf{1}_m)$ is the noise caused by active elements of the m -th HR-RIS. In (25), \mathbf{g}_{lk}^T and $z_{d,k}$ are the effective downlink channel and the aggregated noise at the k -th UE, respectively. Similar to the aggregated noise at APs in the uplink training phase (i.e., see (14)), $z_{d,k}$ has zero-mean and variance $\sigma_{d,k}^2 = \sigma_U^2 + \sum_{m=1}^M \beta_{km}^{\text{SU}} \sum_{n \in \mathcal{A}_m} |\alpha_{mn}|^2 \sigma_S^2$. From (24), $r_{d,k}$ can be expressed as

$$r_{d,k} = \sqrt{\rho_d} \sum_{l=1}^L \left(\sqrt{\eta_{lk}} \mathbf{g}_{lk}^T \hat{\mathbf{g}}_{lk}^* s_k + \sum_{k' \neq k}^K \sqrt{\eta_{lk'}} \mathbf{g}_{lk'}^T \hat{\mathbf{g}}_{lk'}^* s_{k'} \right) + z_{d,k}. \quad (26)$$

B. Uplink Payload Transmission

In the uplink, all K UEs simultaneously send their data to APs. Let q_k with $\mathbb{E}\{|q_k|^2\} = 1$ and ϑ_k with $\vartheta_k \in [0, 1]$ be the symbol and the transmit power coefficient of the k -th UE, respectively. The received signal at the l -th AP is

$$\mathbf{y}_l = \sqrt{\rho_u} \sum_{k=1}^K \sqrt{\vartheta_k} \mathbf{g}_{lk} q_k + \mathbf{z}_{u,l}, \quad (27)$$

where ρ_u is the maximum transmit power at each UE, and $\mathbf{z}_{u,l} \triangleq \mathbf{z}_{A,l} + \sum_{m=1}^M \mathbf{H}_{lm}^{\text{SA}} \Psi_m (\mathbf{z}_{\text{SI},m} + \mathbf{z}_{N,m})$ is the aggregated noise at the l -th AP. Each element of $\mathbf{z}_{u,l}$ has zero-mean and variance $\sigma_{u,l}^2 = \sigma_A^2 + \sum_{m=1}^M \beta_{lm}^{\text{SA}} \sum_{n \in \mathcal{A}_m} |\alpha_{mn}|^2 \sigma_S^2$. Similar to the conventional CF mMIMO systems, the signal vectors received at the APs are combined with the conjugate of the local channel estimates to yield $\{\hat{\mathbf{g}}_{lk}^H \mathbf{y}_l\}$, $\forall l$, which are then sent to the CPU via a backhaul network [1], [62]. To detect the data symbol q_k of the k -th UE at the CPU [63], $\{\hat{\mathbf{g}}_{lk}^H \mathbf{y}_l\}$, $\forall l$ are linearly combined using the weights $\{\omega_{lk}\}$, $\forall l, k$ to obtain

$$r_{u,k} = \sum_{l=1}^L \omega_{lk} \hat{\mathbf{g}}_{lk}^H \mathbf{y}_l = \sum_{k'=1}^K \sum_{l=1}^L \sqrt{\rho_u \vartheta_{k'}} \omega_{lk} \hat{\mathbf{g}}_{lk}^H \mathbf{g}_{lk'} q_{k'} + \sum_{l=1}^L \omega_{lk} \hat{\mathbf{g}}_{lk}^H \mathbf{z}_{u,l}. \quad (28)$$

IV. DOWNLINK AND UPLINK PERFORMANCE ANALYSIS

In this section, we derive the closed-form SE for both the uplink and downlink channels, followed by important observations to characterize the system performance as well as the performance gain offered by HR-RISs.

A. Downlink Spectral Efficiency

1) *Closed-Form Downlink Spectral Efficiency*: Since there are no downlink pilot symbols, UE k treats the mean of the effective channel gain as the true channel for signal detection. This method is widely used in the mMIMO literature [1]. With this method, we rewrite (26) in the following form

$$r_{d,k} = \text{DS}_{d,k} s_k + \text{BU}_{d,k} s_k + \sum_{k' \neq k}^K \text{UI}_{d,kk'} s_{k'} + z_{d,k}, \quad (29)$$

where

$$\begin{aligned} \text{DS}_{d,k} &\triangleq \sqrt{\rho_d} \mathbb{E} \left\{ \sum_{l=1}^L \sqrt{\eta_{lk}} \mathbf{g}_{lk}^T \hat{\mathbf{g}}_{lk}^* \right\}, \\ \text{BU}_{d,k} &\triangleq \sqrt{\rho_d} \left(\sum_{l=1}^L \sqrt{\eta_{lk}} \mathbf{g}_{lk}^T \hat{\mathbf{g}}_{lk}^* - \mathbb{E} \left\{ \sum_{l=1}^L \sqrt{\eta_{lk}} \mathbf{g}_{lk}^T \hat{\mathbf{g}}_{lk}^* \right\} \right), \\ \text{UI}_{d,kk'} &\triangleq \sqrt{\rho_d} \sum_{l=1}^L \sqrt{\eta_{lk'}} \mathbf{g}_{lk'}^T \hat{\mathbf{g}}_{lk}^* \end{aligned}$$

represent the desired signal, beamforming uncertainty gain, and inter-user interference, respectively. The SE of the k -th UE is given by

$$\text{SE}_{d,k} = \frac{\tau_d}{\tau_c} \log_2 (1 + \text{SINR}_{d,k}), \quad (30)$$

where τ_d is the duration of the downlink payload transmission, and

$$\text{SINR}_{d,k} \triangleq \frac{|\text{DS}_{d,k}|^2}{\mathbb{E} \left\{ |\text{BU}_{d,k}|^2 \right\} + \sum_{k' \neq k}^K \mathbb{E} \left\{ |\text{UI}_{d,kk'}|^2 \right\} + \sigma_{d,k}^2}.$$

Theorem 2: In the downlink of the considered HR-RIS-aided CF mMIMO system, the SE of the k -th UE can be

$$\text{SE}_{d,k}(\boldsymbol{\eta}, \boldsymbol{\alpha}) = \frac{\tau_d}{\tau_c} \log_2 \left(1 + \frac{\rho_d |\mathbf{u}_k^T(\boldsymbol{\alpha}) \bar{\boldsymbol{\eta}}_k|^2}{\rho_d \sum_{k' \neq k}^K |\mathbf{v}_{kk'}^T(\boldsymbol{\alpha}) \bar{\boldsymbol{\eta}}_{k'}|^2 + \rho_d \sum_{k'=1}^K \|\mathbf{D}_{kk'}(\boldsymbol{\alpha}) \bar{\boldsymbol{\eta}}_{k'}\|^2 + \sigma_{d,k}^2(\boldsymbol{\alpha})} \right), \quad (31)$$

$$\text{SE}_{d,k}^{\text{iid}}(\boldsymbol{\eta}, \boldsymbol{\alpha}) = \frac{\tau_d}{\tau_c} \log_2 \left(1 + \frac{\rho_d N_A^2 |\bar{\gamma}_k^T(\boldsymbol{\alpha}) \bar{\boldsymbol{\eta}}_k|^2}{\rho_d N_A \sum_{k'=1}^K \|\mathbf{D}_{kk'}(\boldsymbol{\alpha}) \bar{\boldsymbol{\eta}}_{k'}\|^2 + \sigma_{d,k}^2(\boldsymbol{\alpha})} \right), \quad (41)$$

approximated by (31), shown at the top of this page, where $\boldsymbol{\alpha} \triangleq \{\alpha_{mn}\}, \forall m, n, \boldsymbol{\eta} = \{\eta_{lk}\}, \forall l, k$, and

$$\bar{\boldsymbol{\eta}}_k \triangleq [\sqrt{\eta_{1k}}, \dots, \sqrt{\eta_{Lk}}]^T, \quad (32)$$

$$\mathbf{u}_k(\boldsymbol{\alpha}) \triangleq [u_{1k}(\boldsymbol{\alpha}), \dots, u_{Lk}(\boldsymbol{\alpha})]^T, \quad (33)$$

$$\mathbf{v}_{kk'}(\boldsymbol{\alpha}) \triangleq [v_{1kk'}(\boldsymbol{\alpha}), \dots, v_{Lkk'}(\boldsymbol{\alpha})]^T, \quad (34)$$

$$\mathbf{D}_{kk'}(\boldsymbol{\alpha}) \triangleq \text{diag} \left\{ d_{1kk'}^{\frac{1}{2}}(\boldsymbol{\alpha}), \dots, d_{Lkk'}^{\frac{1}{2}}(\boldsymbol{\alpha}) \right\}. \quad (35)$$

Here, the l -th elements of $\mathbf{u}_k(\boldsymbol{\alpha})$, $\mathbf{v}_{kk'}(\boldsymbol{\alpha})$, and $\mathbf{D}_{kk'}(\boldsymbol{\alpha})$, $l = 1, \dots, L$, are defined as

$$u_{lk}(\boldsymbol{\alpha}) \triangleq \text{trace}(\hat{\mathbf{C}}_{lk}) + \|\boldsymbol{\mu}_{lk}\|^2, \quad (36)$$

$$v_{lkk'}(\boldsymbol{\alpha}) \triangleq \boldsymbol{\mu}_{lk}^T \boldsymbol{\mu}_{l'k'}^*, \quad (37)$$

$$d_{lkk'}(\boldsymbol{\alpha}) \triangleq \begin{cases} 2\boldsymbol{\mu}_{lk}^H \hat{\mathbf{C}}_{lk} \boldsymbol{\mu}_{lk} + \text{trace}(\hat{\mathbf{C}}_{lk}^2 + \tilde{\mathbf{R}}_{lk} \circ \hat{\mathbf{R}}_{lk}), & k = k' \\ \boldsymbol{\mu}_{lk}^H \mathbf{C}_{lk} \boldsymbol{\mu}_{l'k'} + \boldsymbol{\mu}_{l'k'}^H \check{\mathbf{C}}_{l'k'} \boldsymbol{\mu}_{lk} + \text{trace}(\mathbf{T}_{lkk'}), & k \neq k', \end{cases} \quad (38)$$

where

$$\mathbf{T}_{lkk'} \triangleq \mathbf{C}_{lk} \circ \hat{\mathbf{C}}_{l'k'} + \tau_p \rho_p \sigma_p^2 \mathbf{R}_{lk} \check{\mathbf{C}}_{l'k'} \mathbf{E}_{lk'}^{-1} (\check{\mathbf{C}}_{l'k'} \mathbf{E}_{l'k'}^{-1})^H, \quad (39)$$

$$\hat{\mathbf{C}}_{lk} \triangleq \tau_p^2 \rho_p^2 \check{\mathbf{C}}_{lk} \mathbf{E}_{lk}^{-1} \left(\sum_{\bar{k}=1}^K |\boldsymbol{\varphi}_{\bar{k}}^H \boldsymbol{\varphi}_{k'}|^2 \mathbf{C}_{l\bar{k}} \right) \mathbf{E}_{lk}^{-H} \check{\mathbf{C}}_{lk}^H, \quad (40)$$

and $\boldsymbol{\mu}_{lk}$, \mathbf{C}_{lk} , \mathbf{E}_{lk} , $\hat{\mathbf{C}}_{lk}$, $\hat{\mathbf{R}}_{lk}$ and $\tilde{\mathbf{R}}_{lk}$ are given in (19)–(23).

Proof: See Appendix B. \square

In Theorem 2, $\bar{\boldsymbol{\eta}}_k$ is determined by the power coefficients associated with the k -th UE; $u_{lk}(\boldsymbol{\alpha})$, $v_{lkk'}(\boldsymbol{\alpha})$, and $d_{lkk'}(\boldsymbol{\alpha})$ are the functions of HR-RIS coefficients ($\boldsymbol{\alpha}$) and large-scale fading parameters, as observed from (18)–(22), (39), (40). Along with $\bar{\boldsymbol{\eta}}_k$, $\mathbf{u}_k(\boldsymbol{\alpha})$ determines the desired signal power, while $\mathbf{v}_{kk'}(\boldsymbol{\alpha})$ and $\mathbf{D}_{kk'}(\boldsymbol{\alpha})$ represent the beamforming uncertainty gain and inter-user interference power, respectively, as shown in (31). We note that (31) is the approximate SE of the k -th UE because of the approximations (B.6), (B.12)–(B.14) in Appendix B. However, the SE in (31) aligns well with that obtained by Monte Carlo simulations, as will be numerically justified in Section V.

Remark 1: If all the channels $\mathbf{h}_{lk}^{\text{UA}}$, $\mathbf{h}_{km}^{\text{US}}$, and $\mathbf{H}_{lm}^{\text{SA}}$ follow independent and identically distributed (i.i.d.) Rayleigh fading model, the SE of the k -th UE can be given as (41) (at the top of this page), where $\bar{\boldsymbol{\gamma}}_k(\boldsymbol{\alpha}) \triangleq [\gamma_{1k}, \dots, \gamma_{Lk}]^T$ and $\mathbf{D}_{kk'}(\boldsymbol{\alpha}) \triangleq$

$\text{diag} \{ \sqrt{\zeta_{1k} \gamma_{1k}}, \dots, \sqrt{\zeta_{Lk} \gamma_{Lk}} \}$ with

$$\zeta_{lk} \triangleq \zeta_{lk}^{\text{UA}} + \sum_{m=1}^M \sum_{n=1}^N |\alpha_{mn}|^2 \zeta_{km}^{\text{US}} \zeta_{lm}^{\text{SA}}, \quad (42)$$

$$\gamma_{lk} \triangleq \frac{\tau_p \rho_p \zeta_{lk}^2}{\tau_p \rho_p \sum_{k'=1}^K |\boldsymbol{\varphi}_{k'}^H \boldsymbol{\varphi}_k|^2 \zeta_{lk'} + \sigma_{p,l}^2}. \quad (43)$$

We omit the proof of Remark 1 because (41) can be obtained by applying $\kappa_{lk}^{\text{UA}} = \kappa_{km}^{\text{US}} = \kappa_{lm}^{\text{SA}} = 0$ and $\mathbf{Q}_{lk}^{\text{A}} = \mathbf{Q}_{lmn}^{\text{A}} = \mathbf{0}_{N_A}, \forall l, m, k$ to Theorem 2.

2) *Power gains of HR-RISs:* First, we note that the SINR in (41) can be re-expressed as

$$\text{SINR}_{d,k}^{\text{iid}} = \frac{\rho_d N_A^2 \left(\sum_{l=1}^L \eta_{lk}^{1/2} \gamma_{lk} \right)^2}{\rho_d N_A \sum_{k'=1}^K \sum_{l=1}^L \eta_{lk} \zeta_{lk} \gamma_{lk'} + \sigma_{d,k}^2(\boldsymbol{\alpha})}. \quad (44)$$

By dividing both the numerator and denominator of $\text{SINR}_{d,k}^{\text{iid}}$ by $L^2 N_A^2$, one can observe that the interference and noise disappear as the total number of transmit antennas grows without bound, i.e., $LN_A \rightarrow \infty$. A similar observation can be made for $L \rightarrow \infty$. Therefore, in the following, we investigate the power of the desired signal to show the power gains of the considered system offered by HR-RISs. More specifically, we analyze how the received desired power at a UE is improved with the HR-RIS active coefficients. To facilitate the analysis, we ignore the channel estimation errors and assume perfect CSI availability.

Remark 2: Under the same assumptions and setup as those in Remark 1, let $P_{d,k}^{\text{HR-RIS}} \triangleq |\text{DS}_{d,k}|^2$ be the received power of the desired signal at the k -th UE in the downlink assisted by HR-RISs. $P_{d,k}^{\text{HR-RIS}}$ is given as

$$P_{d,k}^{\text{HR-RIS}} = P_{d,k}^{\text{direct}} + P_{d,k}^{\text{passive}} + P_{d,k}^{\text{active}} + o_1 (\zeta_{lk}^{\text{UA}} \zeta_{km}^{\text{US}} \zeta_{lm}^{\text{SA}}) + o_2 \left((\zeta_{km}^{\text{US}} \zeta_{lm}^{\text{SA}})^2 \right), \quad (45)$$

where

$$P_{d,k}^{\text{direct}} \triangleq \rho_d N_A^2 \left(\sum_{l=1}^L \zeta_{lk}^{\text{UA}} \eta_{lk}^{\frac{1}{2}} \right)^2,$$

$$P_{d,k}^{\text{passive}} \triangleq \rho_d N_A^2 \left(\sum_{l=1}^L \sum_{m=1}^M \sum_{n \in \mathcal{A}_m} \zeta_{km}^{\text{US}} \zeta_{lm}^{\text{SA}} \eta_{lk}^{\frac{1}{2}} \right)^2,$$

$$P_{d,k}^{\text{active}} \triangleq \rho_d N_A^2 \left(\sum_{l=1}^L \sum_{m=1}^M \sum_{n \in \mathcal{A}_m} |\alpha_{mn}|^2 \zeta_{km}^{\text{US}} \zeta_{lm}^{\text{SA}} \eta_{lk}^{\frac{1}{2}} \right)^2,$$

represent the (desired) signal power at the k -th UE received via

the direct AP-UE link, via reflecting through $N - N_R$ passive elements and relaying through N_R active elements of HR-RISs, respectively. Equivalently, $P_{d,k}^{\text{direct}}$ is the received power in conventional CF mMIMO systems without RIS/HR-RIS, while $P_{d,k}^{\text{direct}} + P_{d,k}^{\text{passive}} + o_1 (\zeta_{lk}^{\text{UA}} \zeta_{km}^{\text{US}} \zeta_{lm}^{\text{SA}}) + o_2 \left((\zeta_{km}^{\text{US}} \zeta_{lm}^{\text{SA}})^2 \right)$ is the received power in passive RISs-assisted systems. We note that the last two terms in (45) are very small and negligible compared to the others due to the multiplicative path loss coefficients. It is observed from (45) that HR-RISs provide the k -th UE with a power gain of $P_{d,k}^{\text{active}}$ compared to the conventional passive RISs.

Remark 2 can be shown via a straightforward expansion of $P_{d,k}^{\text{HR-RIS}} = \rho_d N_A \left(\sum_{l=1}^L \gamma_{lk} \eta_{lk}^{\frac{1}{2}} \right)^2$, with the note that $\gamma_{lk} = \zeta_{lk}$ under the assumption of perfect CSI and ζ_{lk} given in (43). With the presence of CSI error, we still have $\gamma_{lk} \approx \zeta_{lk}$, especially at high SNRs and when the pilot contamination effect is small. Specifically, this can be seen by rewriting the denominator of (43) as $\tau_p \rho_p \zeta_{lk} + \tau_p \rho_p \sum_{k' \neq k} |\varphi_{k'}^H \varphi_k|^2 \zeta_{lk'} + \sigma_{p,l}^2$, which is approximately equal to $\tau_p \rho_p \zeta_{lk}$ when $|\varphi_{k'}^H \varphi_k|^2 \ll 1$ and $\sigma_{p,l}^2 \ll \tau_p \rho_p \zeta_{lk}$, i.e., at high SNRs. This is reasonable because under these conditions, the CSI error becomes negligible.

Remark 3: Consider an extreme scenario in which the received signal over the direct AP-UE link is very weak that it is negligible compared to the others (due to low ρ_d and/or large ζ_{lk}^{UA}), resulting in $P_{d,k}^{\text{direct}} \approx 0$. Furthermore, when the active elements of HR-RISs are provided with a sufficiently large power budget, we have $P_{d,k}^{\text{active}} \gg P_{d,k}^{\text{passive}}$. Thus, we can write

$$P_{d,k}^{\text{HR-RIS}} \approx \rho_d N_A^2 \left(\sum_{l=1}^L \eta_{lk}^{\frac{1}{2}} \sum_{m=1}^M \zeta_{km}^{\text{US}} \zeta_{lm}^{\text{SA}} \sum_{n \in \mathcal{A}_m} |\alpha_{mn}|^2 \right)^2. \quad (46)$$

Here, it is worth noting that $\zeta_{km}^{\text{US}} \zeta_{lm}^{\text{SA}}$ reflects the multiplicative fading that occurs on the reflecting channels. For a sufficiently large power budget at the HR-RISs, it follows that $\zeta_{km}^{\text{US}} \zeta_{lm}^{\text{SA}} \sum_{n \in \mathcal{A}_m} |\alpha_{mn}|^2 \geq 1$ (i.e., the multiplicative path loss is eliminated), while this cannot be attained by conventional passive RISs with $|\alpha_{mn}|^2 = 1, \forall m, n$.

Although the conclusions in Remarks 2 and 3 are made for the scenario of the weak LoS and direct links, they are generally valid for CF mMIMO systems where APs and UEs are deployed in a large area. It is obvious from (45) and (46) that the more the power budget at HR-RISs and/or the more deployed HR-RISs, the better the system performance can be achieved. The impact of the power budget at HR-RIS and number of HR-RISs to the SE performance will be further justified by numerical results in Section V.

B. Uplink Spectral Efficiency

In the uplink, APs send their combined signals to the CPU, where the desired symbol q_k is detected from $r_{u,k}$ in (28). We assume that the CPU uses only statistical knowledge of the channel to perform signal detection [1]. We rewrite (28)

in the following form:

$$r_{u,k} = \text{DS}_{u,k} q_k + \text{BU}_{u,k} q_k + \sum_{k' \neq k}^K \text{UI}_{u,kk'} q_{k'} + \tilde{z}_{u,k},$$

where

$$\begin{aligned} \text{DS}_{u,k} &\triangleq \sqrt{\rho_u \vartheta_k} \mathbb{E} \left\{ \sum_{l=1}^L \omega_{lk} \hat{\mathbf{g}}_{lk}^H \mathbf{g}_{lk} \right\}, \\ \text{BU}_{u,k} &\triangleq \sqrt{\rho_u \vartheta_k} \left(\sum_{l=1}^L \omega_{lk} \hat{\mathbf{g}}_{lk}^H \mathbf{g}_{lk} - \mathbb{E} \left\{ \sum_{l=1}^L \omega_{lk} \hat{\mathbf{g}}_{lk}^H \mathbf{g}_{lk} \right\} \right), \\ \text{UI}_{u,kk'} &\triangleq \sqrt{\rho_u \vartheta_{k'}} \sum_{l=1}^L \omega_{lk'} \hat{\mathbf{g}}_{lk'}^H \mathbf{g}_{lk'}, \end{aligned}$$

are the desired signal, beamforming uncertainty gain, and inter-user interference, respectively, and $\tilde{z}_{u,k} \triangleq \sum_{l=1}^L \omega_{lk} \hat{\mathbf{g}}_{lk}^H \mathbf{z}_{u,l}$. As a result, we can derive the uplink SE of the k -th UE as (47) (at the top of the next page).

Theorem 3: In the uplink of the considered HR-RIS-aided CF mMIMO system with matched filtering detection, the SE of the k -th UE can be approximated by (48), shown at the top of the next page, where $\boldsymbol{\omega} \triangleq \{\omega_k\}, \forall k$ with $\omega_k \triangleq [\omega_{1k}, \dots, \omega_{Lk}]^T$, and $\mathbf{u}_k(\boldsymbol{\alpha}), \mathbf{v}_{kk'}(\boldsymbol{\alpha})$, and $\mathbf{D}_{kk'}(\boldsymbol{\alpha})$ are given in (33)–(35), respectively, and $\boldsymbol{\Sigma}_k(\boldsymbol{\alpha}) \triangleq \text{diag} \left\{ \sigma_{u,1} \sqrt{u_{1k}(\boldsymbol{\alpha})}, \dots, \sigma_{u,L} \sqrt{u_{Lk}(\boldsymbol{\alpha})} \right\}$.

Proof: See Appendix C. \square

To further confirm that the closed-form expression of $\text{SE}_{u,k}(\boldsymbol{\vartheta}, \boldsymbol{\omega}, \boldsymbol{\alpha})$ in (48) is also valid for the conventional CF mMIMO uplink system, we consider the simple case where all the channels $\mathbf{h}_{lk}^{\text{UA}}, \mathbf{h}_{km}^{\text{US}}$, and $\mathbf{H}_{lm}^{\text{SA}}$ follow i.i.d. Rayleigh fading model and assume $\omega_{lk} = 1, \forall l, k$. In this case, the SE of the k -th UE in the uplink can be given as (49) (at the top of the next page), which is in an agreement with the result in [1] by applying $\varphi_k^H \varphi_{k'} = 0, \forall k \neq k'$ to (27) (in [1]) and fixing $N_A = 1$ in (49) for single-antenna APs.

The discussions and conclusions in Section IV-A2 are also valid for the uplink channel. Specifically, from (49), it is clear that as $LN_A \rightarrow \infty$ or $L \rightarrow \infty$, the received signal becomes free of interference and noise. Note that the received power of the desired signal (i.e., the numerator of the SINR in (49)) has the same form as in (41) by setting $\eta_{lk} = \vartheta_k, \forall l$. Then, the conclusions on the power gains provided by HR-RISs in Remarks 2 and 3 still hold for the uplink channel.

V. SIMULATION RESULTS

In this section, we provide numerical results to verify the analytical derivations and demonstrate the merits of the HR-RIS-sided CF mMIMO system. For comparison purposes, we also include the performance of the conventional CF mMIMO system with and without passive RISs.

A. Simulation Setup

We denote by (x_l^A, y_l^A) and (x_k^U, y_k^U) the positions in a 2D coordinate of the l -th AP and the k -UE, respectively. We consider the following two scenarios:

$$\text{SE}_{u,k} = \frac{\tau_u}{\tau_c} \log_2 \left(1 + \frac{|\text{DS}_{u,k}|^2}{\mathbb{E} \{ |\text{BU}_{u,k}|^2 \} + \sum_{k' \neq k}^K \mathbb{E} \{ |\text{UI}_{u,kk'}|^2 \} + \mathbb{E} \{ |\tilde{z}_{u,k}|^2 \} } \right), \quad (47)$$

$$\text{SE}_{u,k}(\boldsymbol{\vartheta}, \boldsymbol{\omega}, \boldsymbol{\alpha}) = \frac{\tau_u}{\tau_c} \log_2 \left(1 + \frac{\rho_u \vartheta_k |\mathbf{u}_k(\boldsymbol{\alpha})^T \boldsymbol{\omega}_k|^2}{\rho_u \sum_{k' \neq k}^K \vartheta_{k'} |\mathbf{v}_{kk'}^T(\boldsymbol{\alpha}) \boldsymbol{\omega}_{k'}|^2 + \rho_u \sum_{k'=1}^K \vartheta_{k'} \|\mathbf{D}_{kk'}(\boldsymbol{\alpha}) \boldsymbol{\omega}_{k'}\|^2 + \|\boldsymbol{\Sigma}_k(\boldsymbol{\alpha}) \boldsymbol{\omega}_k\|^2} \right), \quad (48)$$

$$\text{SE}_{u,k}^{\text{iid}}(\boldsymbol{\vartheta}, \boldsymbol{\alpha}) = \frac{\tau_u}{\tau_c} \log_2 \left(1 + \frac{\rho_u \vartheta_k N_A^2 \left(\sum_{l=1}^L \gamma_{lk} \right)^2}{\rho_u N_A \sum_{k'=1}^K \vartheta_{k'} \sum_{l=1}^L \zeta_{lk} \gamma_{lk'} + N_A \sum_{l=1}^L \sigma_{u,l}^2 \gamma_{lk}(\boldsymbol{\alpha})} \right), \quad (49)$$

- \mathcal{S}_1 : APs and UEs are randomly distributed over the entire coverage area of $1 \times 1 \text{ km}^2$, i.e., $x_l^A, y_l^A, x_k^U, y_k^U \in [-0.5, 0.5] \text{ km}$, $\forall l, k$ [1], [2].
- \mathcal{S}_2 : APs and UEs are randomly distributed in two adjacent sub-regions such that $x_l^A, y_l^A \in [-0.5, 0] \text{ km}$, and $x_k^U, y_k^U \in [0, 0.5] \text{ km}$, $\forall l, k$.

In both scenarios \mathcal{S}_1 and \mathcal{S}_2 , RISs/HR-RISs are randomly deployed inside circles of a radius of 10 m centred by the UEs, implying that RISs/HR-RISs are in the vicinity of the UEs.

Let $d \in \{d_{lk}^{\text{UA}}, d_{km}^{\text{US}}, d_{lm}^{\text{SA}}\}$ be the distance between the l -th AP and k -th UE, between the k -th UE and the m -th HR-RIS, and between the m -th HR-RIS and the l -th AP, respectively. The large-scale fading coefficients $\zeta \in \{\zeta_{lk}^{\text{UA}}, \zeta_{km}^{\text{US}}, \zeta_{lm}^{\text{SA}}\}$ are modeled based on the three-slope path loss model in [1], [2], [41], [61], [62], i.e.,

$$\zeta = \begin{cases} \zeta_0 - 35 \log_{10}(d), & \text{if } d > d_1, \\ \zeta_0 - 15 \log_{10}(d_1) - 20 \log_{10}(d), & \text{if } d_0 < d \leq d_1, \\ \zeta_0 - 15 \log_{10}(d_1) - 20 \log_{10}(d_0), & \text{if } d \leq d_0, \end{cases} \quad (50)$$

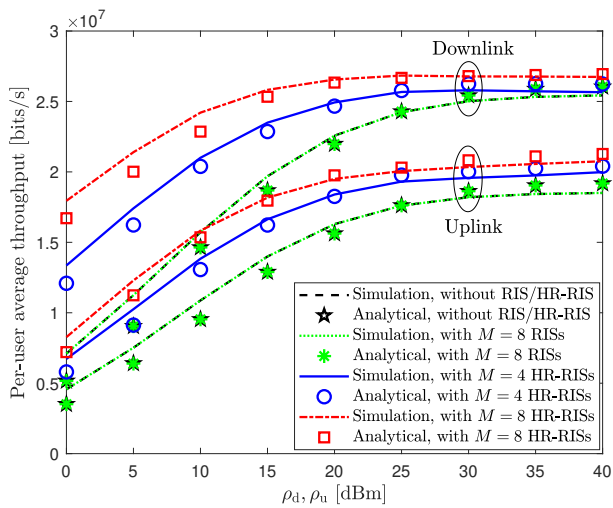
where $\zeta_0 = -140.7 + \text{SF}$ dB with $\text{SF} \sim \mathcal{CN}(0, \sigma_{\text{SF}})$ representing the shadowing factor. In the following simulations, we set $\sigma_{\text{SF}} = 8$ dB, $d_0 = 10$ m, and $d_1 = 50$ m [1], [2]. The Rician factor $\kappa \in \{\kappa_{lk}^{\text{UA}}, \kappa_{km}^{\text{US}}, \kappa_{lm}^{\text{SA}}\}$ is set to $\kappa = P_{\text{LoS}}(d)/(1 - P_{\text{LoS}}(d))$ [64], where $P_{\text{LoS}}(d)$ is the LoS probability given as $P_{\text{LoS}}(d) = \min(\frac{18}{d}, 1) (1 - \exp(-\frac{d}{36})) + \exp(-\frac{d}{36})$ based on the 3GPP-UMa model [65].

We assume the uniform linear arrays (ULAs) for APs and uniform planar arrays (UPAs) for HR-RISs with antenna/element spacing of $d_A \lambda$ and 0.5λ , respectively, where λ is the wave length. Consequently, the LoS channels are modeled as $\bar{\mathbf{h}}_{lk}^{\text{UA}} = \mathbf{a}_{\text{ULA}}(\varpi_{lk}^A)$, $\bar{\mathbf{h}}_{lkm}^{\text{US}} = \mathbf{a}_{\text{UPA}}(\varpi_{lkm}^H, \phi_{lkm}^H)$, and $\bar{\mathbf{h}}_{lm}^{\text{SA}} = \mathbf{a}_{\text{ULA}}(\varpi_{lm}^A) \mathbf{a}_{\text{UPA}}^H(\varpi_{lkm}^H, \phi_{lkm}^H)$, where $\mathbf{a}_{\text{ULA}}(\varpi_{lk}^A)$ and $\mathbf{a}_{\text{UPA}}(\varpi_{lkm}^H, \phi_{lkm}^H)$ are the array response vectors at AP and HR-RIS, with the n -th element given as $a_{\text{ULA},n}(\varpi_{lk}^A) = \exp(j2\pi d_A(n-1) \sin \varpi_{lk}^A)$ and $a_{\text{UPA},n}(\varpi_{lkm}^H, \phi_{lkm}^H) = \exp(j\pi(\lfloor \frac{n}{N_x} \rfloor \sin \varpi_{lkm}^H \sin \phi_{lkm}^H + (n - \lfloor \frac{n}{N_x} \rfloor N_x) \sin \varpi_{lkm}^H \cos \phi_{lkm}^H))$, $n = 1, \dots, N_A$,

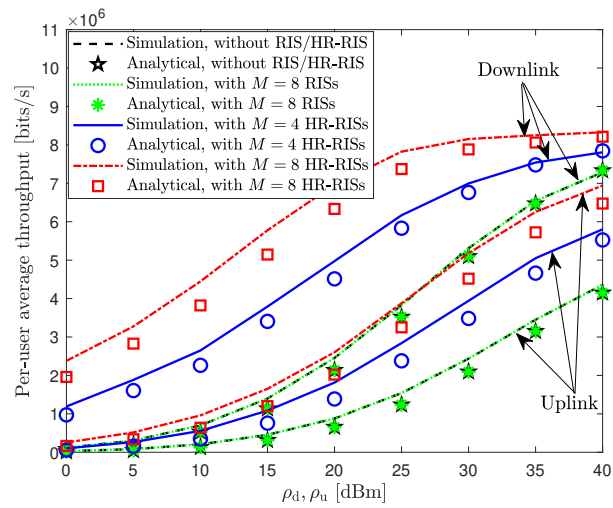
respectively. Here, ϖ_{lk}^A and $\varpi_{lkm}^H \in [0, 2\pi)$ denote the angle-of-departure (AoD) at APs and the azimuth angle-of-arrival (AoA) at HR-RISs, respectively, and $\phi_{lkm}^H \in [-\pi/2, \pi/2)$ denotes the elevation AoA at HR-RISs. We recall that the NLoS channels are modeled by Rayleigh fading, and we assume the Gaussian local scattering model for spatial correlation. Thus, the (i, j) -th entry of \mathbf{Q}_{lk}^A is given as $q_{lk,ij}^A = \frac{1}{\sqrt{2\pi}\sigma_\phi} \int_{-\infty}^{+\infty} \exp(j2\pi d_A(i-j) \sin(\varpi_{lk}^A + \delta)) \exp(-\frac{\delta^2}{2\sigma_\phi^2}) d\delta$, where $\delta \sim \mathcal{N}(0, \sigma_\phi^2)$ is a deviation from ϖ_{lk}^A with angular standard deviation σ_ϕ [56], [57]. Entries of \mathbf{Q}_{lmn}^A are generated similarly. In the simulations, we set $\sigma_\phi = 30^\circ$ for a moderate spatial correlation [57].

Since the optimization of power and reflecting/relaying coefficients is beyond the scope of this paper, we adopt simple equal power control schemes for both downlink and uplink transmissions to obtain $\{\eta_{lk}\}$, $\{\vartheta_k\}$, $\{\alpha_{mn}\}$ [1], [2]. In particular, we assume that the power coefficients of APs are computed based on the large-scale fading of the direct AP-UE channel, i.e., $\eta_{lk} = \left(\sum_{k'=1}^K (N_A \gamma_{lk'}^{\text{UA}} + \|\boldsymbol{\mu}_{lk'}^{\text{UA}}\|^2) \right)^{-1}$, $\forall l, k$, in the downlink transmission, and $\vartheta_k = 1$, $\forall k$ in the uplink transmission [1], [2]. The phases $\{\theta_{mn}\}$ are randomly generated, while the amplitude $\{|\alpha_{mn}|\}$, $n \in \mathcal{A}_m$ of the active elements are obtained based on exhaustive search such that the total transmit power of each HR-RIS is limited by a given power budget ρ_S and equally shared among the active elements. Here, the positions of active elements are randomly generated for all HR-RISs. Furthermore, we assume that at the CPU, the local estimates from all APs are equally weighted, i.e., $\omega_{lk} = 1$, $\forall l, k$ [1]. Compared to the conventional passive RIS, each HR-RIS requires an additional power budget ρ_S . In the simulations, the transmit power at each AP in the downlink or at each UE in the uplink of the systems with HR-RISs is reduced by an amount of $\frac{M\rho_S}{L}$ or $\frac{M\rho_S}{K}$, respectively. As a result, the total transmit power (of the transmitters and HR-RISs) in these systems becomes $L(\rho_d - \frac{M\rho_S}{L}) + M\rho_S = L\rho_d$ in the downlink and $K(\rho_u - \frac{M\rho_S}{L}) + M\rho_S = K\rho_u$ in the uplink, which are equal to those of the systems without HR-RIS and with passive RISs.

The noise power is computed as $\sigma_A^2 = \sigma_U^2 = \sigma_N^2 = -170 +$



(a) Scenario \mathcal{S}_1



(b) Scenario \mathcal{S}_2

Fig. 2. Average per-user downlink and uplink throughput of HR-RIS-assisted CF mMIMO systems versus ρ_d and ρ_u with $L = 30$, $N_A = 4$, $K = 4$, $M = \{4, 8\}$, $N = 40$, $N_R = 1$, and $\rho_S = -5$ dBm for both \mathcal{S}_1 and \mathcal{S}_2 .

$10 \log_{10}(B_0) + NF$ (dBm), where we set the system bandwidth $B_0 = 20$ MHz and the noise figure $NF = 9$ dB. Unless otherwise stated, we set the normalized residual SI power to 1 dB, $\tau_c = 200$, $\tau_p = K/2$, $\tau_d = \tau_u = (\tau_c - \tau_p)/2$, and $\rho_p = 100$ mW following studies in [1], [58], [59]. In the simulations, the analytical results are averaged over 100 large-scale channel realizations, while the results obtained by Monte Carlo simulations are averaged out over 1000 small-scale channel realizations.

B. Results and Discussions

In the following simulations, we evaluate the per-user throughput (in bits/s) of the considered schemes, which is obtained by scaling the SE (in bits/s/Hz) with the system bandwidth of $B_0 = 20 \times 10^6$ Hz. We first validate the closed-form expressions of the downlink and uplink SE provided in Theorems 2 and 3, respectively. Fig. 2 shows the down-

link/uplink throughput obtained by analytical derivations and those obtained by Monte Carlo simulations for two considered scenarios \mathcal{S}_1 and \mathcal{S}_2 . The simulation parameters for both scenarios are $L = 30$, $N_A = 4$, $K = 4$, $M = \{4, 8\}$, $N = 40$, $N_R = 1$, and $\rho_S = -5$ dBm. From Fig. 2, the interesting observations are in order:

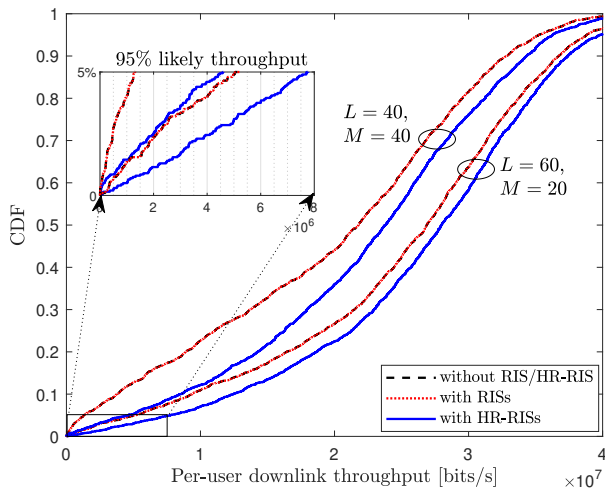
- In all the considered schemes and scenarios, the theoretical results align well with the simulation ones based on Monte Carlo method in the entire considered range of ρ_d and ρ_u , validating the derivations in Theorems 2 and 3.
- With random phase shifts, passive RISs offer marginal performance gain for CF mMIMO systems. We note from (31) that the RIS phase shifts only affect the SE performance via $\mu_{lk}, \forall l, k$. Thus, their performance gain is generally limited, especially with random phase shifts.
- Comparing the throughput of CF mMIMO systems with and without HR-RISs, the former clearly outperforms the latter for all the considered values of ρ_d and ρ_u . In particular, the proposed schemes offer higher gains in \mathcal{S}_2 compared with those in \mathcal{S}_1 , which agrees with the discussion in Remark 3. Furthermore, it is clear that a larger M leads to a more significant improvement in the throughput.
- Finally, we observe that although the throughput gain offered by HR-RISs in the uplink is still noticeable, its improvement is less significant than in the downlink. This is because in the uplink, HR-RISs are placed far away from the receivers (i.e., APs).

To verify the analytical results for a larger scale system, we consider in Table I a CF mMIMO system with $L = 80$, $N_A = 4$, $K = 20$, $M = 20$, and $\rho_d = 200$ mW [1]. The results in Table I show that the downlink throughput obtained by (31) for systems without RISs/HR-RISs, with passive RISs, and with HR-RISs are tight with the simulation ones in both \mathcal{S}_1 and \mathcal{S}_2 . Therefore, in the following, we omit the results of Monte Carlo simulations and focus on large-scale downlink systems with fixed $\rho_d = 200$ mW.

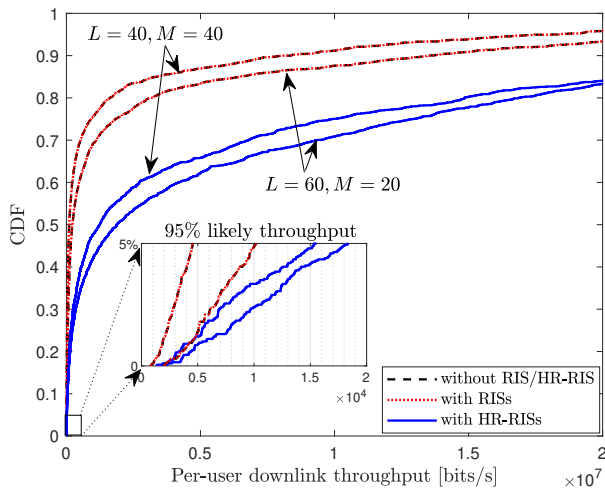
Fig. 3 plots the cumulative distribution functions (CDFs) of per-user throughput of the downlink system with $(L, M) = \{(60, 20), (40, 40)\}$, $N_A = 4$, $K = 20$, $N = 40$, $N_R = 1$, and $\rho_S = -5$ dBm. The results clearly show the advantage of using HR-RISs in both \mathcal{S}_1 and \mathcal{S}_2 . In particular, the system assisted by HR-RISs outperforms the conventional systems, i.e., CF mMIMO systems without any RISs/HR-RISs and with only the passive RISs, in both median and 95%-likely performance, especially when fewer APs are deployed in the network. Specifically, with $(L, M) = (40, 40)$, the 95%-likely per-user downlink throughputs of the conventional systems are only $\{1.25 \times 10^6, 4.53 \times 10^3\}$ bits/s, whereas those of the proposed HR-RIS-aided systems are $\{4.58 \times 10^6, 1.55 \times 10^4\}$ bits/s, implying $\{3.66, 3.42\}$ times improvement in $\{\mathcal{S}_1, \mathcal{S}_2\}$, respectively. With $(L, M) = (60, 20)$, the corresponding gains are nearly $\{1.5, 1.8\}$ times. Furthermore, it can be seen that HR-RIS-aided systems provide more uniform and better performance for all users. These observations confirm the benefits of deploying HR-RISs, especially in an extreme scenario like \mathcal{S}_2 and/or when the number of APs is not large enough.

Table I. Average per-user downlink throughput of CF mMIMO systems without (w/o) RIS/HR-RIS, with M RISs, and with M HR-RISs. The simulation parameters are $L = 80$, $N_A = 4$, $K = 20$, $M = 20$, $N_R = 1$, $\rho_d = 200$ mW, and $\rho_S = -5$ dBm.

Downlink throughput	in \mathcal{S}_1 (Mbits/s)			in \mathcal{S}_2 (Mbits/s)		
	w/o RIS/HR-RIS	with RIS	with HR-RIS	w/o RIS/HR-RIS	with RIS	with HR-RIS
Simulation	25.92	25.95	26.15	4.14	4.15	6.35
Analytical	26.47	26.48	27.12	3.91	3.91	6.32



(a) Scenario \mathcal{S}_1

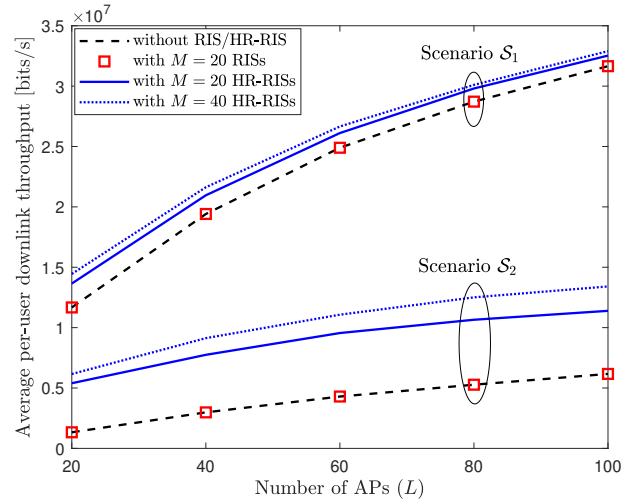


(b) Scenario \mathcal{S}_2

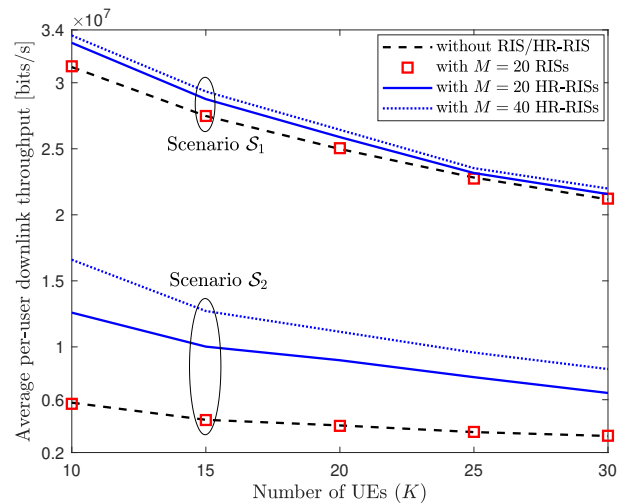
Fig. 3. CDF of downlink per-user throughput with $(L, M) = \{(60, 40), (20, 40)\}$, $N_A = 4$, $K = 20$, $N = 40$, $N_R = 1$, $\rho_d = 200$ mW, and $\rho_S = -5$ dBm for both \mathcal{S}_1 and \mathcal{S}_2 .

In Fig. 4, we investigate the significance of HR-RISs for CF mMIMO systems with different numbers of APs and UEs. To this end, we set $L \in [20, 100]$, $N_A = 4$, $K = 20$, $M = \{20, 40\}$ in Fig. 4(a) and $L = 80$, $K \in [10, 30]$, $M = \{20, 40\}$ in Fig. 4(b). The other parameters are $N_A = 4$, $N = 40$, $N_R = 1$, $\rho_d = 200$ mW, and $\rho_S = -5$ dBm, which are the same for both Figs. 4(a) and 4(b).

Similar to the observations in the previous figures, it is



(a) $L = \{20, \dots, 100\}$, $K = 20$, $M = \{20, 40\}$



(b) $L = 80$, $K = \{10, \dots, 30\}$, $M = \{20, 40\}$

Fig. 4. Average per-user downlink throughput of CF mMIMO systems versus (a) L and (b) K . Other parameters are $N_A = 4$, $N = 40$, $N_R = 1$, $\rho_d = 200$ mW, and $\rho_S = -5$ dBm for both Figs. (a) and (b).

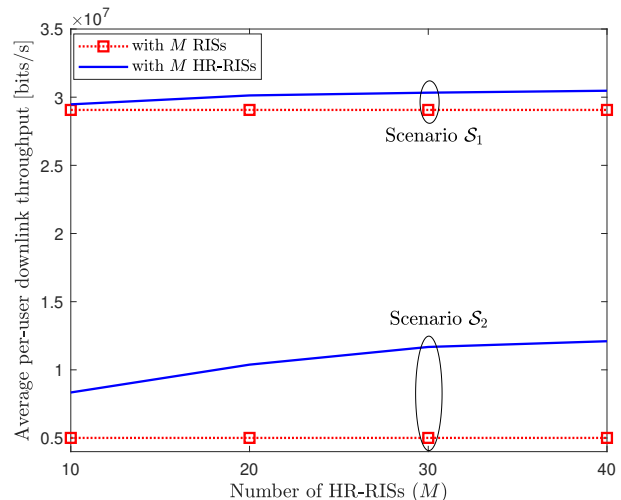
observed in Fig. 4(a) that the performance improvement of the passive RISs is still negligible. In contrast, it can be seen in \mathcal{S}_2 that HR-RISs offer a significant improvement in throughput compared to the system without HR-RISs, even when a very large number of APs are deployed in the system. However, the gain of HR-RISs in \mathcal{S}_1 is not as significant as in \mathcal{S}_2 and reduces when L increases. This is reasonable because when UEs are served by more and closer APs (in

\mathcal{S}_1), HR-RISs become less important. In contrast, when the APs are not always close to the UEs (as in \mathcal{S}_2), deploying more APs just provides marginal performance improvements, while HR-RISs are necessary to assist communications between APs and UEs to greatly improve the system performance, as seen in \mathcal{S}_2 . This result further confirms the discussion in Remark 3. Furthermore, we observe in \mathcal{S}_2 that without HR-RISs, $L = 100$ APs only provide the throughput of around 6 Mbits/s, which can be easily attained by a HR-RIS-aided CF mMIMO systems with 20 APs and 20 HR-RISs. In other words, for a target throughput of 6 Mbits/s, deploying 20 HR-RISs help reduce a large number of APs. This may result in a significant improvement in the system EE because an AP generally requires much higher power consumption than a HR-RIS. Thus, for a good SE-EE tradeoff, it is beneficial to deploy HR-RISs in the system.

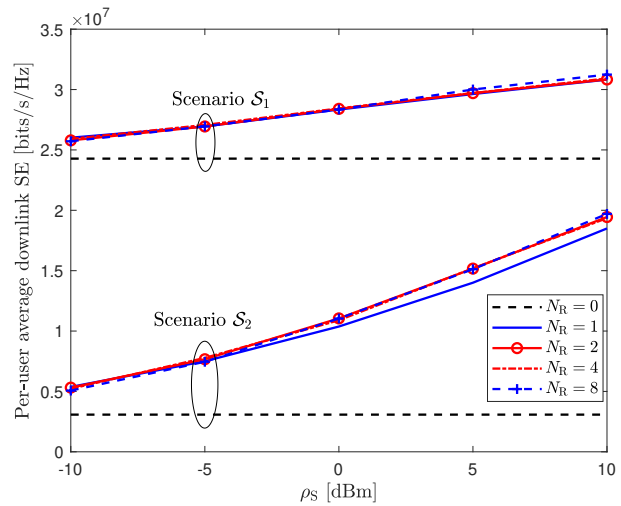
In Fig. 4(b), HR-RIS-aided systems outperform the conventional ones in the entire considered range of K , especially in \mathcal{S}_2 . This is similar to the observations from the previous figures. Furthermore, it is seen that as K increases, the gain offered by the HR-RIS reduces. This is reasonable because when the number of users increases but the number of HR-RISs is fixed, on one hand, more and more users are not supported by HR-RISs, on the other hand, the inter-user interference increase. Consequently, not only the average throughput but also the gain of HR-RISs are reduced.

In Fig. 5, we investigate the impact of various deployments and setups of the HR-RISs. Specifically, we show the performance improvement of the systems with different numbers of HR-RISs in Fig. 5(a) with $L = 80$, $N_A = 4$, $K = 20$, $M \in [10, 40]$, $N_R = 1$, and $\rho_S = -5$ dBm. It is seen that as M increases, i.e., more HR-RISs/RISs are deployed to the network, the throughput of the HR-RIS-assisted system remarkably increases, which is, in contrast, not seen for the conventional passive RISs. It is noteworthy that even when the HR-RISs are sparse (e.g., for the case $M < K = 20$), the throughput gain offered by HR-RISs is still significant. Furthermore, as M increases, the throughput gain of the HR-RISs is more significant in \mathcal{S}_2 than in \mathcal{S}_1 . For example, if each UE has one nearby HR-RIS (e.g., $M = K = 20$), the throughput in is improved by about 5 Mbits/s in \mathcal{S}_2 compared to 1 Mbits/s in \mathcal{S}_1 .

In the previous figures, we considered $N_R = 1$ and $\rho_S = -5$ dBm, which means that each HR-RIS is deployed with only a single active element and a limited power budget so that its increase in the total power consumption is marginal compared to the conventional passive RIS. In Fig. 5(b), we show the impact of the number of active elements and the transmit power of each HR-RIS on the throughput performance, with $N_R = \{0, 1, 2, 4, 8\}$, $\rho_S \in [-10, 10]$ dBm, $L = 30$, $N_A = 4$, $K = 4$, $M = 4$, and $N = 40$. As can be seen, the throughput increases rapidly as ρ_S increases. Unsurprisingly, compared to the case of $N_R = 0$ (i.e., the passive RISs), HR-RISs only require a single or a few active elements to achieve significant improvement in throughput, even with small ρ_S . It is also seen that increasing the number of active elements does not guarantee a significant performance improvement. The reason is that when more active elements are employed, each of them



(a) $L = 80$, $K = 20$, $M = \{10, \dots, 40\}$, $\rho_S = -5$ dBm



(b) $L = 30$, $K = 4$, $M = 5$, $\rho_S = \{-10, \dots, 10\}$ dBm

Fig. 5. Average per-user downlink throughput of HR-RIS-aided CF mMIMO systems versus (a) M and (b) ρ_S . Other parameters are $N = 40$ and $\rho_d = 200$ mW for both Figs. (a) and (b).

shares a smaller power amplification gain. This is particularly true when an equal power allocation among the active elements of the HR-RISs is assumed. In particular, if ρ_S is very limited, increasing N_R can cause performance degradation as seen for $\rho_S \leq -5$ dBm in Fig. 5(b). Similar observations can be found in [7]. This further advocates a practical implementation of the proposed HR-RIS design, where only a small number of active elements is needed considering its limited power budget.

In Figs. 2–5, we have investigated the performance of RIS/HR-RIS-aided CF mMIMO systems under the three-slope path loss model. In Fig. 6, we consider the case that the path loss is modeled by the COST 321 Walfish-Ikegami model as in [55]–[57], [66], [67]. Specifically, the probability of having an LoS path in the channel between the l -th AP and the k -th UE with distance d_{lk}^{UA} is given by $P_{\text{LoS}}(d_{lk}^{UA}) = 1 - d_{lk}^{UA}/300$ if $0 < d_{lk}^{UA} < 300$ m and otherwise $P_{\text{LoS}}(d_{lk}^{UA}) = 0$. The corresponding Rician factor is computed as $\kappa_{lk}^{UA} = 10^{1.3 - 0.003d_{lk}^{UA}}$

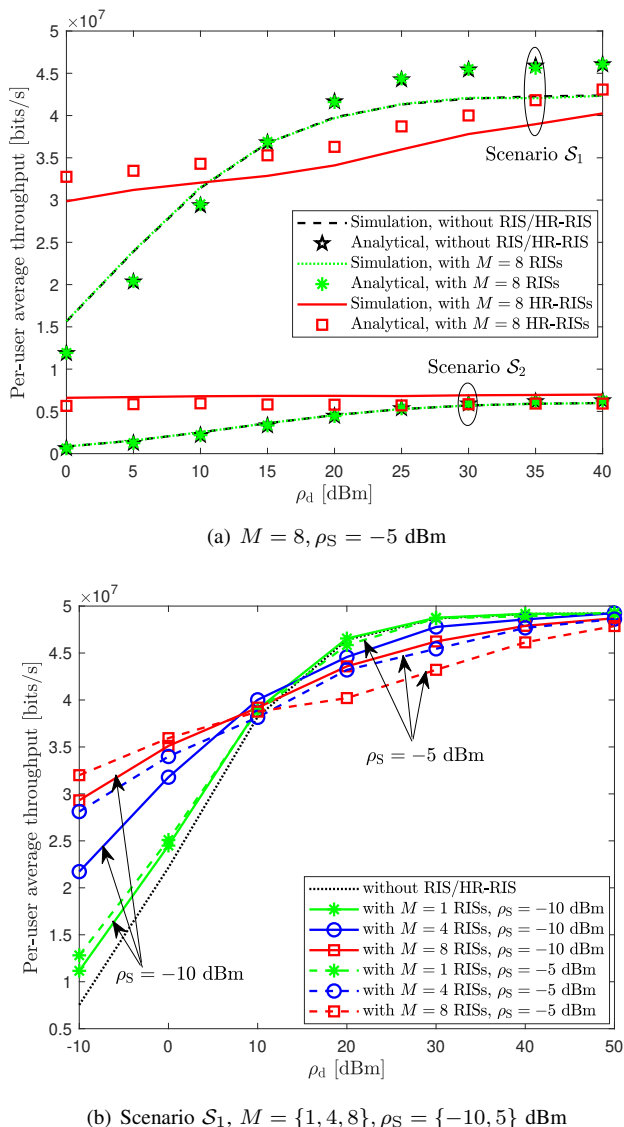


Fig. 6. Average per-user downlink throughput of HR-RIS-assisted CF mMIMO systems with the COST 321 Walfish-Ikegami path loss model. We set $L = 30$, $N_A = 4$, $K = 4$, $M = \{1, 4, 8\}$, $N = 40$, $N_R = 1$, and $\rho_S = \{-5, -10\}$ dBm.

if the LoS component exists and otherwise $\kappa_{lk}^{\text{UA}} = 0$. Then, the path loss ζ_{lk}^{UA} (in dB) is modeled as

$$\zeta_{lk}^{\text{UA}} = \begin{cases} -30.18 - 26 \log_{10}(d_{lk}/1 \text{ m}) + \text{SF}_{lk}, & \kappa_{lk} \neq 0 \\ -34.53 - 38 \log_{10}(d_{lk}/1 \text{ m}) + \text{SF}_{lk}, & \kappa_{lk} = 0 \end{cases}, \quad (51)$$

where $\text{SF}_{lk} = \sqrt{\varkappa} a_l + \sqrt{1 - \varkappa} b_k$ represents the shadowing factor, with \varkappa being the shadow fading parameter, and $a_l, b_k \sim \mathcal{CN}(0, \sigma_{\text{SF}}^2)$. We consider correlated shadowing coefficients with covariance functions $\mathbb{E}\{a_l a_{l'}\} = 2^{-\frac{d_{ll'}}{d_{\text{dc}}}}$ and $\mathbb{E}\{b_k b_{k'}\} = 2^{-\frac{d_{kk'}}{d_{\text{dc}}}}$, where $d_{ll'}$ and $d_{kk'}$ are the distances between the l -th and l' -th APs and between the k -th and k' -th UEs, respectively. We set $\sigma_{\text{SF}} = 8$ dB, $\varkappa = 0.5$, $d_{\text{dc}} = 100$ m [56], [57], and $\{\kappa_{km}^{\text{US}}, \kappa_{lm}^{\text{SA}}\}$, $\{\zeta_{km}^{\text{US}}, \zeta_{lm}^{\text{SA}}\}$ are modeled similarly.

In Fig. 6(a), we show the downlink throughput obtained

by analytical derivations and those obtained by Monte Carlo simulations for both scenarios \mathcal{S}_1 and \mathcal{S}_2 with path loss model (51). The simulation parameters are the same as those in Fig. 2. It is seen that the analytical results are still good approximations of those obtained via Monte Carlo simulations in both scenarios. The HR-RISs provide significant performance improvement in \mathcal{S}_2 , especially at low and moderate ρ_d . However, it is interesting to see that in \mathcal{S}_1 , the HR-RISs cause performance loss at high ρ_d . This is because with the COST 321 Walfish-Ikegami model, the path loss becomes less severe, and thus, the gain from signal amplification of the HR-RISs is less significant while the interference is large.

We further investigate the interesting observation on the performance of the HR-RISs in \mathcal{S}_1 with the COST 321 Walfish-Ikegami model in Fig. 6(b) for various values of ρ_S and M . Specifically, we consider $\rho_S = \{-10, -5\}$ dBm, $M = \{1, 4, 8\}$, and the other parameters are the same as in Fig. 6(a). It is seen that for $\rho_d \leq 10$ dBm, a larger M and higher ρ_S always lead to a better SE, and the gains offered by HR-RISs in this regime are significant. In contrast, for $\rho_d > 10$ dBm, less HR-RISs with low power budget (i.e., smaller M and lower ρ_S) should be employed. These observations motivate further designs and optimizations of the considered HR-RISs-aided CF mMIMO systems with focuses on power allocation and HR-RIS selection/on-off schemes.

VI. CONCLUSION

This work has considered the novel HR-RIS-aided CF mMIMO system in which HR-RISs are equipped with both active relay and passive reflecting elements to assist communications between multiple APs and UEs. We have modeled the uplink and downlink channels of the considered system and derived the MMSE estimate of the effective channels. Then, we have provided closed-form expressions for the uplink and downlink SE. In addition, the power scaling effects and performance gains over conventional systems have also been discussed to provide more insights into the proposed HR-RIS design. The analytical derivations have been numerically justified by simulations, showing that the performance improvement in terms of per-user SE offered by HR-RISs in both the uplink and downlink can be significant when the transmit power of APs is low and/or when UEs are located far away from APs. In the case that the direct communications links between the users and APs are strong, and the APs' transmit power is high, the gain is generally limited. They have also contributed to the realization of an efficient and practical implementation of the proposed HR-RIS design that requires only a few active elements to guarantee low costs of hardware and power consumption. Our analytical results in this work also call for more efficient transmission strategies and intelligent end-to-end resource allocation policies. A similar analysis of the HR-RIS-aided CF mMIMO systems employing other centralized/distributed processing approaches is a potential extension of this work. In particular, the extensions taking into account the estimation of phase shifts of LoS components and spatial correlation among HR-RIS elements are interesting topics for our future works. Furthermore, finding the best

trade-offs in terms of energy efficiency with power budgets at the transmitters and HR-RISs is also an important future research topic.

APPENDIX A
PROOF OF THEOREM 1

The MMSE estimate of \mathbf{g}_{lk} is computed as

$$\hat{\mathbf{g}}_{lk} = \mathbb{E}\{\mathbf{g}_{lk}\} + \mathbb{C}\{\mathbf{g}_{lk}, \mathbf{y}_{lk}\} \mathbb{C}\{\mathbf{y}_{lk}\}^{-1} (\mathbf{y}_{lk} - \mathbb{E}\{\mathbf{y}_{lk}\}). \quad (\text{A.1})$$

To this end, we compute the required statistical quantities in (A.1) to derive $\hat{\mathbf{g}}_{lk}$. First, from (8), we have

$$\mathbb{E}\{\mathbf{g}_{lk}\} = \boldsymbol{\mu}_{lk}^{\text{UA}} + \sum_{m=1}^M \sum_{n=1}^N \alpha_{mn} \bar{\boldsymbol{\mu}}_{lkmn}^{\text{USA}} \triangleq \boldsymbol{\mu}_{lk}, \quad (\text{A.2})$$

where $\bar{\boldsymbol{\mu}}_{lkmn}^{\text{USA}} \triangleq \boldsymbol{\mu}_{lkmn}^{\text{SA}} \boldsymbol{\mu}_{lkmn}^{\text{US}}$. Noting that $\mathbb{E}\{\tilde{\mathbf{z}}_{lk}\} = \mathbf{0}$ and from (15), we obtain

$$\begin{aligned} \mathbb{E}\{\mathbf{y}_{lk}\} &= \mathbb{E}\left\{\sqrt{\tau_p \rho_p} \mathbf{g}_{lk} + \sqrt{\tau_p \rho_p} \sum_{k' \neq k} \mathbf{g}_{lk'} \boldsymbol{\varphi}_{k'}^H \boldsymbol{\varphi}_k + \tilde{\mathbf{z}}_{lk}\right\} \\ &= \sqrt{\tau_p \rho_p} \sum_{k'=1}^K \boldsymbol{\varphi}_{k'}^H \boldsymbol{\varphi}_k \boldsymbol{\mu}_{lk'}. \end{aligned} \quad (\text{A.3})$$

To compute $\mathbb{C}\{\mathbf{g}_{lk}, \mathbf{y}_{lk}\}$, from $\mathbf{y}_{lk} = \sqrt{\tau_p \rho_p} \mathbf{g}_{lk} + \sqrt{\tau_p \rho_p} \sum_{k' \neq k} \mathbf{g}_{lk'} \boldsymbol{\varphi}_{k'}^H \boldsymbol{\varphi}_k + \tilde{\mathbf{z}}_{lk}$, we have

$$\begin{aligned} \mathbb{C}\{\mathbf{g}_{lk}, \mathbf{y}_{lk}\} &= \sqrt{\tau_p \rho_p} \mathbb{C}\{\mathbf{g}_{lk}\} + \mathbb{C}\{\mathbf{g}_{lk}, \tilde{\mathbf{z}}_{lk}\} \\ &\quad + \sqrt{\tau_p \rho_p} \sum_{k' \neq k} \mathbb{C}\{\mathbf{g}_{lk}, \mathbf{g}_{lk'}\} \boldsymbol{\varphi}_{k'}^H \boldsymbol{\varphi}_k \\ &\stackrel{\text{(a)}}{=} \sqrt{\tau_p \rho_p} \mathbf{C}_{lk} + \sqrt{\tau_p \rho_p} \sum_{k' \neq k} \boldsymbol{\varphi}_{k'}^H \boldsymbol{\varphi}_k \mathbf{C}_{lkk'} \\ &= \sqrt{\tau_p \rho_p} \left(\mathbf{C}_{lk} + \sum_{k' \neq k} \boldsymbol{\varphi}_{k'}^H \boldsymbol{\varphi}_k \mathbf{C}_{lkk'} \right). \end{aligned} \quad (\text{A.4})$$

where $\mathbf{C}_{lk} \triangleq \mathbb{C}\{\mathbf{g}_{lk}\}$ and $\mathbf{C}_{lkk'} \triangleq \mathbb{C}\{\mathbf{g}_{lk}, \mathbf{g}_{lk'}\}$. Equality (a) can be obtained by expanding $\mathbb{C}\{\mathbf{g}_{lk}, \tilde{\mathbf{z}}_{lk}\} = \mathbb{E}\{\mathbf{g}_{lk} \tilde{\mathbf{z}}_{lk}^H\} - \mathbb{E}\{\mathbf{g}_{lk}\} \mathbb{E}\{\tilde{\mathbf{z}}_{lk}\}^H = \mathbf{0}_{N_A}$ due to $\mathbb{E}\{\mathbf{g}_{lk} \tilde{\mathbf{z}}_{lk}^H\} = \mathbf{0}_{N_A}$ and $\mathbb{E}\{\tilde{\mathbf{z}}_{lk}\} = \mathbf{0}$ as the noise entries/elements of $\mathbf{Z}_{A,l}$, $\mathbf{z}_{SI,mn}$ and $\mathbf{z}_{N,mn}$ are independent of \mathbf{g}_{lk} and have zero means $\forall l, m, n$. Furthermore, in (A.4), \mathbf{C}_{lk} can be computed based on (8), as

$$\begin{aligned} \mathbf{C}_{lk} &= \mathbb{C}\{\mathbf{g}_{lk}\} \\ &= \mathbb{C}\left\{\mathbf{h}_{lk}^{\text{UA}}\right\} + \sum_{m=1}^M \sum_{n=1}^N |\alpha_{mn}|^2 \mathbb{C}\left\{\mathbf{h}_{lkmn}^{\text{SA}} \mathbf{h}_{lkmn}^{\text{US}}\right\}, \end{aligned} \quad (\text{A.5})$$

where $\mathbb{C}\left\{\mathbf{h}_{lk}^{\text{UA}}\right\} = \beta_{lk}^{\text{UA}} \mathbf{Q}_{lk}^{\text{A}}$ and

$$\begin{aligned} \mathbb{C}\left\{\mathbf{h}_{lkmn}^{\text{SA}} \mathbf{h}_{lkmn}^{\text{US}}\right\} &= \mathbb{E}\left\{\mathbf{h}_{lkmn}^{\text{SA}} \mathbf{h}_{lkmn}^{\text{US}} (\mathbf{h}_{lkmn}^{\text{US}})^* (\mathbf{h}_{lkmn}^{\text{SA}})^H\right\} \\ &\quad - \mathbb{E}\left\{\mathbf{h}_{lkmn}^{\text{SA}} \mathbf{h}_{lkmn}^{\text{US}}\right\} \mathbb{E}\left\{(\mathbf{h}_{lkmn}^{\text{US}})^* (\mathbf{h}_{lkmn}^{\text{SA}})^H\right\} \\ &\stackrel{\text{(b)}}{=} \mathbb{E}\left\{|\mathbf{h}_{lkmn}^{\text{US}}|^2\right\} \mathbb{E}\left\{\mathbf{h}_{lkmn}^{\text{SA}} (\mathbf{h}_{lkmn}^{\text{SA}})^H\right\} \\ &\quad - |\mathbb{E}\{\mathbf{h}_{lkmn}^{\text{US}}\}|^2 \mathbb{E}\left\{\mathbf{h}_{lkmn}^{\text{SA}}\right\} \mathbb{E}\left\{\mathbf{h}_{lkmn}^{\text{SA}}\right\}^H \\ &\stackrel{\text{(c)}}{=} \left(\beta_{km}^{\text{US}} + |\mu_{kmn}^{\text{US}}|^2\right) \left(\beta_{lm}^{\text{SA}} \mathbf{Q}_{lkmn}^{\text{A}} + \boldsymbol{\mu}_{lkmn}^{\text{SA}} (\boldsymbol{\mu}_{lkmn}^{\text{SA}})^H\right) \\ &\quad - |\mu_{kmn}^{\text{US}}|^2 \boldsymbol{\mu}_{lkmn}^{\text{SA}} (\boldsymbol{\mu}_{lkmn}^{\text{SA}})^H \end{aligned}$$

$$= \left(\beta_{km}^{\text{US}} + |\mu_{kmn}^{\text{US}}|^2\right) \beta_{lm}^{\text{SA}} \mathbf{Q}_{lkmn}^{\text{A}} + \beta_{km}^{\text{US}} \boldsymbol{\mu}_{lkmn}^{\text{SA}} (\boldsymbol{\mu}_{lkmn}^{\text{SA}})^H. \quad (\text{A.6})$$

Here, equality (b) is obtained because $\mathbf{h}_{lkmn}^{\text{SA}}$ and $\mathbf{h}_{lkmn}^{\text{US}}$ are independent, and equality (c) follows $\mathbb{E}\left\{|\mathbf{h}_{lkmn}^{\text{US}}|^2\right\} = \beta_{km}^{\text{US}} + |\mu_{kmn}^{\text{US}}|^2$ and $\mathbb{E}\left\{\mathbf{h}_{lkmn}^{\text{SA}} (\mathbf{h}_{lkmn}^{\text{SA}})^H\right\} = \beta_{lm}^{\text{SA}} \mathbf{Q}_{lkmn}^{\text{A}} + \boldsymbol{\mu}_{lkmn}^{\text{SA}} (\boldsymbol{\mu}_{lkmn}^{\text{SA}})^H$. Thus, we obtain

$$\begin{aligned} \mathbf{C}_{lk} &= \beta_{lk}^{\text{UA}} \mathbf{Q}_{lk}^{\text{A}} + \sum_{m=1}^M \sum_{n=1}^N |\alpha_{mn}|^2 \left(\beta_{km}^{\text{US}} + |\mu_{kmn}^{\text{US}}|^2\right) \beta_{lm}^{\text{SA}} \mathbf{Q}_{lkmn}^{\text{A}} \\ &\quad + \beta_{km}^{\text{US}} \boldsymbol{\mu}_{lkmn}^{\text{SA}} (\boldsymbol{\mu}_{lkmn}^{\text{SA}})^H. \end{aligned}$$

Furthermore, we can compute $\mathbf{C}_{lkk'}$ in (A.4) based on (8) as (A.7)–(A.9) (at the top of the next page), where equality (d) follows $\mathbb{C}\left\{\mathbf{h}_{lk}^{\text{UA}}, \mathbf{h}_{lk'}^{\text{UA}}\right\} = \mathbb{C}\left\{\mathbf{h}_{lk}^{\text{UA}}, \mathbf{h}_{lkmn}^{\text{SA}} \mathbf{h}_{lkmn}^{\text{US}}\right\} = \mathbb{C}\left\{\mathbf{h}_{lkmn}^{\text{SA}} \mathbf{h}_{lkmn}^{\text{US}}, \mathbf{h}_{lk'}^{\text{UA}}\right\} = \mathbf{0}_{N_A}$ because $\mathbf{h}_{lk}^{\text{UA}}$ is uncorrelated with $\mathbf{h}_{lk'}^{\text{UA}}$ and $\mathbf{h}_{lkmn}^{\text{SA}} \mathbf{h}_{lkmn}^{\text{US}}$, $\forall k \neq k'$. The result in (A.8) follows the derivations in equality (c) of (A.6) and the fact that $\{h_{k'm'n'}^{\text{US}}, h_{k'm'n}^{\text{US}}, h_{l'm'n'}^{\text{SA}}, h_{l'm'n}^{\text{SA}}\}$ are mutually independent. Equality (e) in (A.9) follows the independence of $\mathbf{h}_{lkmn}^{\text{SA}}$ and $\mathbf{h}_{lkmn}^{\text{US}}$, $\forall k$. From (A.7)–(A.9), we obtain

$$\mathbf{C}_{lkk'} = \sum_{m=1}^M \sum_{n=1}^N |\alpha_{mn}|^2 \mu_{k'mn}^{\text{US}} (\mu_{k'mn}^{\text{US}})^* \beta_{lm}^{\text{SA}} \mathbf{Q}_{lkmn}^{\text{A}}.$$

In addition, we have

$$\begin{aligned} \mathbb{E}\{\mathbf{g}_{lk} \mathbf{g}_{lk}^H\} &= \mathbf{C}_{lk} + \boldsymbol{\mu}_{lk} \boldsymbol{\mu}_{lk}^H \triangleq \mathbf{R}_{lk}, \\ \mathbb{E}\{\|\mathbf{g}_{lk}\|^2\} &= \text{trace}(\mathbf{R}_{lk}) = \text{trace}(\mathbf{C}_{lk}) + \|\boldsymbol{\mu}_{lk}\|^2, \end{aligned} \quad (\text{A.10})$$

which are useful for the subsequent derivations. $\mathbb{C}\{\mathbf{y}_{lk}\}$ can be computed based on (15) as

$$\begin{aligned} \mathbb{C}\{\mathbf{y}_{lk}\} &= \mathbb{C}\left\{\sqrt{\tau_p \rho_p} \mathbf{g}_{lk} + \sqrt{\tau_p \rho_p} \sum_{k' \neq k} \mathbf{g}_{lk'} \boldsymbol{\varphi}_{k'}^H \boldsymbol{\varphi}_k + \tilde{\mathbf{z}}_{lk}\right\} \\ &= \tau_p \rho_p \sum_{k'=1}^K |\boldsymbol{\varphi}_{k'}^H \boldsymbol{\varphi}_k|^2 \mathbf{C}_{lkk'} + \sigma_{p,l}^2 \mathbf{I}_{N_A}. \end{aligned} \quad (\text{A.11})$$

Finally, by substituting the results in (A.2), (A.3), (A.4), and (A.11) into (A.1), we obtain

$$\begin{aligned} \hat{\mathbf{g}}_{lk} &= \boldsymbol{\mu}_{lk} + \sqrt{\tau_p \rho_p} \left(\mathbf{C}_{lk} + \sum_{k' \neq k} \boldsymbol{\varphi}_{k'}^H \boldsymbol{\varphi}_k \mathbf{C}_{lkk'} \right) \\ &\quad \times \left[\tau_p \rho_p \sum_{k'=1}^K |\boldsymbol{\varphi}_{k'}^H \boldsymbol{\varphi}_k|^2 \mathbf{C}_{lkk'} + \sigma_{p,l}^2 \mathbf{I}_{N_A} \right]^{-1} \\ &\quad \times \left(\mathbf{y}_{lk} - \sqrt{\tau_p \rho_p} \sum_{k'=1}^K \boldsymbol{\varphi}_{k'}^H \boldsymbol{\varphi}_k \boldsymbol{\mu}_{lk'} \right). \end{aligned}$$

For ease of exposition, let us denote

$$\begin{aligned} \check{\boldsymbol{\mu}}_{lk} &\triangleq \sum_{k'=1}^K \boldsymbol{\varphi}_{k'}^H \boldsymbol{\varphi}_k \boldsymbol{\mu}_{lk'}, \quad \check{\mathbf{C}}_{lk} \triangleq \mathbf{C}_{lk} + \sum_{k' \neq k} \boldsymbol{\varphi}_{k'}^H \boldsymbol{\varphi}_k \mathbf{C}_{lkk'}, \\ \mathbf{E}_{lk} &\triangleq \tau_p \rho_p \left(\sum_{k'=1}^K |\boldsymbol{\varphi}_{k'}^H \boldsymbol{\varphi}_k|^2 \mathbf{C}_{lkk'} \right) + \sigma_{p,l}^2 \mathbf{I}_{N_A} = \mathbb{C}\{\mathbf{y}_{lk}\}. \end{aligned}$$

$$\begin{aligned}
\mathbf{C}_{lkk'} &= \mathbb{C} \left\{ \mathbf{h}_{lk}^{\text{UA}} + \sum_{m=1}^M \sum_{n=1}^N \alpha_{mn} \mathbf{h}_{lmn}^{\text{SA}} h_{kmn}^{\text{US}}, \mathbf{h}_{lk'}^{\text{UA}} + \sum_{m=1}^M \sum_{n=1}^N \alpha_{mn} \mathbf{h}_{lmn}^{\text{SA}} h_{k'mn}^{\text{US}} \right\} \\
&= \mathbb{C} \left\{ \mathbf{h}_{lk}^{\text{UA}}, \mathbf{h}_{lk'}^{\text{UA}} \right\} + \sum_{m=1}^M \sum_{n=1}^N \alpha_{mn} \mathbb{C} \left\{ \mathbf{h}_{lk}^{\text{UA}}, \mathbf{h}_{lmn}^{\text{SA}} h_{k'mn}^{\text{US}} \right\} + \sum_{m=1}^M \sum_{n=1}^N \alpha_{mn} \mathbb{C} \left\{ \mathbf{h}_{lmn}^{\text{SA}} h_{kmn}^{\text{US}}, \mathbf{h}_{lk'}^{\text{UA}} \right\} \\
&\quad + \mathbb{C} \left\{ \sum_{m=1}^M \sum_{n=1}^N \alpha_{mn} \mathbf{h}_{lmn}^{\text{SA}} h_{kmn}^{\text{US}}, \sum_{m=1}^M \sum_{n=1}^N \alpha_{mn} \mathbf{h}_{lmn}^{\text{SA}} h_{k'mn}^{\text{US}} \right\} \\
&\stackrel{\text{(d)}}{=} \mathbb{C} \left\{ \sum_{m=1}^M \sum_{n=1}^N \alpha_{mn} \mathbf{h}_{lmn}^{\text{SA}} h_{kmn}^{\text{US}}, \sum_{m=1}^M \sum_{n=1}^N \alpha_{mn} \mathbf{h}_{lmn}^{\text{SA}} h_{k'mn}^{\text{US}} \right\} = \mathbf{E}_{lkk',1} - \mathbf{E}_{lkk',2}, \tag{A.7} \\
\mathbf{E}_{lkk',1} &= \mathbb{E} \left\{ \left(\sum_{m=1}^M \sum_{n=1}^N \alpha_{mn} \mathbf{h}_{lmn}^{\text{SA}} h_{kmn}^{\text{US}} \right) \left(\sum_{m=1}^M \sum_{n=1}^N \alpha_{mn}^* (h_{k'mn}^{\text{US}})^* (\mathbf{h}_{lmn}^{\text{SA}})^H \right) \right\} \\
&= \sum_{m=1}^M \sum_{n=1}^N |\alpha_{mn}|^2 \mathbb{E} \{ h_{kmn}^{\text{US}} \} \mathbb{E} \{ h_{k'mn}^{\text{US}} \}^* \mathbb{E} \left\{ \mathbf{h}_{lmn}^{\text{SA}} (\mathbf{h}_{lmn}^{\text{SA}})^H \right\} \\
&\quad + \sum_{m',n',\bar{m},\bar{n}} \sum_{(m',n',\bar{m},\bar{n}) \neq (m,n,m,n)} \alpha_{m'n'} \alpha_{\bar{m}\bar{n}}^* \mathbb{E} \left\{ h_{km'n'}^{\text{US}} (h_{k'\bar{m}\bar{n}}^{\text{US}})^* \mathbf{h}_{lm'n'}^{\text{SA}} (\mathbf{h}_{l\bar{m}\bar{n}}^{\text{SA}})^H \right\} \\
&= \sum_{m=1}^M \sum_{n=1}^N |\alpha_{mn}|^2 \mu_{kmn}^{\text{US}} (\mu_{k'mn}^{\text{US}})^* \left(\beta_{lm}^{\text{SA}} \mathbf{Q}_{lmn}^{\text{A}} + \boldsymbol{\mu}_{lmn}^{\text{SA}} (\boldsymbol{\mu}_{lmn}^{\text{SA}})^H \right) \\
&\quad + \sum_{m',n',\bar{m},\bar{n}} \sum_{(m',n',\bar{m},\bar{n}) \neq (m,n,m,n)} \alpha_{m'n'} \alpha_{\bar{m}\bar{n}}^* \mu_{km'n'}^{\text{US}} (\mu_{k'\bar{m}\bar{n}}^{\text{US}})^* \boldsymbol{\mu}_{lm'n'}^{\text{SA}} (\boldsymbol{\mu}_{l\bar{m}\bar{n}}^{\text{SA}})^H, \tag{A.8} \\
\mathbf{E}_{lkk',2} &= \mathbb{E} \left\{ \sum_{m=1}^M \sum_{n=1}^N \alpha_{mn} \mathbf{h}_{lmn}^{\text{SA}} h_{kmn}^{\text{US}} \right\} \left(\mathbb{E} \left\{ \sum_{m=1}^M \sum_{n=1}^N \alpha_{mn} \mathbf{h}_{lmn}^{\text{SA}} h_{k'mn}^{\text{US}} \right\} \right)^H \\
&\stackrel{\text{(e)}}{=} \left(\sum_{m=1}^M \sum_{n=1}^N \alpha_{mn} \boldsymbol{\mu}_{lmn}^{\text{SA}} \mu_{kmn}^{\text{US}} \right) \left(\sum_{m=1}^M \sum_{n=1}^N \alpha_{mn}^* (\boldsymbol{\mu}_{lmn}^{\text{SA}})^H (\mu_{k'mn}^{\text{US}})^* \right)^H \\
&= \sum_{m=1}^M \sum_{n=1}^N |\alpha_{mn}|^2 \mu_{kmn}^{\text{US}} (\mu_{k'mn}^{\text{US}})^* \boldsymbol{\mu}_{lmn}^{\text{SA}} (\boldsymbol{\mu}_{lmn}^{\text{SA}})^H \\
&\quad + \sum_{m',n',\bar{m},\bar{n}} \sum_{(m',n',\bar{m},\bar{n}) \neq (m,n,m,n)} \alpha_{m'n'} \alpha_{\bar{m}\bar{n}}^* \mu_{km'n'}^{\text{US}} (\mu_{k'\bar{m}\bar{n}}^{\text{US}})^* \boldsymbol{\mu}_{lm'n'}^{\text{SA}} (\boldsymbol{\mu}_{l\bar{m}\bar{n}}^{\text{SA}})^H, \tag{A.9}
\end{aligned}$$

Then, we can express $\hat{\mathbf{g}}_{lk}$ as

$$\begin{aligned}
\hat{\mathbf{g}}_{lk} &= \boldsymbol{\mu}_{lk} + \sqrt{\tau_p \rho_p} \check{\mathbf{C}}_{lk} \mathbf{E}_{lk}^{-1} (\mathbf{y}_{lk} - \sqrt{\tau_p \rho_p} \check{\boldsymbol{\mu}}_{lk}) \\
&= \boldsymbol{\mu}_{lk} - \tau_p \rho_p \check{\mathbf{C}}_{lk} \mathbf{E}_{lk}^{-1} \check{\boldsymbol{\mu}}_{lk} + \sqrt{\tau_p \rho_p} \check{\mathbf{C}}_{lk} \mathbf{E}_{lk}^{-1} \mathbf{y}_{lk}. \tag{A.12}
\end{aligned}$$

We have $\mathbb{E} \{ \hat{\mathbf{g}}_{lk} \} = \boldsymbol{\mu}_{lk}$ from (A.1), and $\mathbb{C} \{ \hat{\mathbf{g}}_{lk} \} = \tau_p \rho_p \check{\mathbf{C}}_{lk} \mathbf{E}_{lk}^{-1} \mathbb{C} \{ \mathbf{y}_{lk} \} (\check{\mathbf{C}}_{lk} \mathbf{E}_{lk}^{-1})^H = \tau_p \rho_p \check{\mathbf{C}}_{lk} \mathbf{E}_{lk}^{-H} \check{\mathbf{C}}_{lk}^H \triangleq \hat{\mathbf{C}}_{lk}$ from (A.11) and (A.12). Besides, by using $\mathbb{C} \{ \hat{\mathbf{g}}_{lk} \} = \mathbb{E} \{ \hat{\mathbf{g}}_{lk} \hat{\mathbf{g}}_{lk}^H \} - \mathbb{E} \{ \hat{\mathbf{g}}_{lk} \} \mathbb{E} \{ \hat{\mathbf{g}}_{lk} \}^H$, $\mathbb{E} \{ \hat{\mathbf{g}}_{lk} \hat{\mathbf{g}}_{lk}^H \}$ and $\mathbb{E} \{ \|\hat{\mathbf{g}}_{lk}\|^2 \}$ are obtained as in (22). The estimation error is given by $\tilde{\mathbf{g}}_{lk} = \mathbf{g}_{lk} - \hat{\mathbf{g}}_{lk}$. Because $\mathbb{E} \{ \mathbf{g}_{lk} \} = \mathbb{E} \{ \hat{\mathbf{g}}_{lk} \} = \boldsymbol{\mu}_{lk}$, it is clear that $\mathbb{E} \{ \tilde{\mathbf{g}}_{lk} \} = \mathbf{0}$, and thus, $\mathbb{C} \{ \tilde{\mathbf{g}}_{lk} \} = \mathbb{E} \{ \tilde{\mathbf{g}}_{lk} \tilde{\mathbf{g}}_{lk}^H \} = \mathbf{C}_{lk} - \hat{\mathbf{C}}_{lk} \triangleq \tilde{\mathbf{R}}_{lk}$, as given in Theorem 1.

APPENDIX B PROOF OF THEOREM 2

We now compute $|\text{DS}_{d,k}|^2$, $\mathbb{E} \{ |\text{BU}_{d,k}|^2 \}$, and $\mathbb{E} \{ |\text{UI}_{kk'}|^2 \}$ to show the closed-form of $\text{SE}_{d,k}$ in (31).

1) Compute $|\text{DS}_{d,k}|^2$: First, by recalling that $\mathbf{g}_{lk} = \tilde{\mathbf{g}}_{lk} + \hat{\mathbf{g}}_{lk}$ and that $\tilde{\mathbf{g}}_{lk}$ and $\hat{\mathbf{g}}_{lk}$ are uncorrelated, we have

$$\begin{aligned}
\text{DS}_{d,k} &= \sqrt{\rho_d} \sum_{l=1}^L \sqrt{\eta_{lk}} \mathbb{E} \{ \mathbf{g}_{lk}^T \hat{\mathbf{g}}_{lk}^* \} \\
&= \sqrt{\rho_d} \sum_{l=1}^L \sqrt{\eta_{lk}} \mathbb{E} \{ (\tilde{\mathbf{g}}_{lk} + \hat{\mathbf{g}}_{lk})^T \hat{\mathbf{g}}_{lk}^* \} \\
&= \sqrt{\rho_d} \sum_{l=1}^L \sqrt{\eta_{lk}} \left(\mathbb{E} \{ \tilde{\mathbf{g}}_{lk}^T \hat{\mathbf{g}}_{lk}^* \} + \mathbb{E} \{ \|\hat{\mathbf{g}}_{lk}\|^2 \} \right) \\
&= \sqrt{\rho_d} \sum_{l=1}^L \sqrt{\eta_{lk}} \left(\underbrace{\text{trace}(\hat{\mathbf{C}}_{lk}) + \|\boldsymbol{\mu}_{lk}\|^2}_{\triangleq u_{lk}(\boldsymbol{\alpha})} \right), \tag{B.1}
\end{aligned}$$

where the last equality follows (22) and $\mathbb{E} \{ \tilde{\mathbf{g}}_{lk} \} = \mathbf{0}$. By defining two vectors $\bar{\boldsymbol{\eta}}_k \triangleq [\sqrt{\eta_{1k}}, \dots, \sqrt{\eta_{Lk}}]^T$ and $\mathbf{u}_k(\boldsymbol{\alpha}) \triangleq [u_{1k}(\boldsymbol{\alpha}), \dots, u_{Lk}(\boldsymbol{\alpha})]^T$, we can write

$$|\text{DS}_{d,k}|^2 = \rho_d |\mathbf{u}_k(\boldsymbol{\alpha})^T \bar{\boldsymbol{\eta}}_k|^2. \tag{B.2}$$

2) Compute $\mathbb{E}\{|\text{BU}_{d,k}|^2\}$: We rewrite

$$\begin{aligned} \text{BU}_{d,k} &= \sqrt{\rho_d} \left(\sum_{l=1}^L \sqrt{\eta_{lk}} \mathbf{g}_{lk}^T \hat{\mathbf{g}}_{lk}^* - \mathbb{E} \left\{ \sum_{l=1}^L \sqrt{\eta_{lk}} \mathbf{g}_{lk}^T \hat{\mathbf{g}}_{lk}^* \right\} \right) \\ &= \sqrt{\rho_d} \sum_{l=1}^L \sqrt{\eta_{lk}} \left(\mathbf{g}_{lk}^T \hat{\mathbf{g}}_{lk}^* - \mathbb{E} \left\{ \mathbf{g}_{lk}^T \hat{\mathbf{g}}_{lk}^* \right\} \right) \end{aligned}$$

Then, $\mathbb{E}\{|\text{BU}_{d,k}|^2\}$ can be computed as

$$\begin{aligned} \mathbb{E}\{|\text{BU}_{d,k}|^2\} &= \rho_d \mathbb{E} \left\{ \left| \sum_{l=1}^L \sqrt{\eta_{lk}} \left(\mathbf{g}_{lk}^T \hat{\mathbf{g}}_{lk}^* - \mathbb{E} \left\{ \mathbf{g}_{lk}^T \hat{\mathbf{g}}_{lk}^* \right\} \right) \right|^2 \right\} \\ &= \rho_d \sum_{l=1}^L \eta_{lk} \mathbb{E} \left\{ \left| \mathbf{g}_{lk}^T \hat{\mathbf{g}}_{lk}^* - \mathbb{E} \left\{ \mathbf{g}_{lk}^T \hat{\mathbf{g}}_{lk}^* \right\} \right|^2 \right\} \\ &\quad + \rho_d \sum_{l=1}^L \sum_{l' \neq l}^L \sqrt{\eta_{lk} \eta_{l'k}} (r_{l'k} + r_{l'k}^*), \quad (\text{B.3}) \end{aligned}$$

where

$$r_{l'k} \triangleq \mathbb{E} \left\{ \left(\mathbf{g}_{lk}^T \hat{\mathbf{g}}_{lk}^* - \mathbb{E} \left\{ \mathbf{g}_{lk}^T \hat{\mathbf{g}}_{lk}^* \right\} \right) \left(\mathbf{g}_{l'k}^T \hat{\mathbf{g}}_{l'k}^* - \mathbb{E} \left\{ \mathbf{g}_{l'k}^T \hat{\mathbf{g}}_{l'k}^* \right\} \right)^* \right\}.$$

By using $\mathbf{g}_{lk} = \tilde{\mathbf{g}}_{lk} + \hat{\mathbf{g}}_{lk}$, $\mathbb{E}\{\tilde{\mathbf{g}}_{lk}\} = \mathbf{0}$, and the fact that $\tilde{\mathbf{g}}_{lk}$ and $\hat{\mathbf{g}}_{lk}$ are uncorrelated, we obtain

$$\begin{aligned} r_{l'k} &= \mathbb{E} \left\{ \|\hat{\mathbf{g}}_{lk}\|^2 \|\hat{\mathbf{g}}_{l'k}\|^2 \right\} - \mathbb{E} \left\{ \|\hat{\mathbf{g}}_{lk}\|^2 \right\} \mathbb{E} \left\{ \|\hat{\mathbf{g}}_{l'k}\|^2 \right\} \\ &= \mathbb{C} \left\{ \|\hat{\mathbf{g}}_{lk}\|^2, \|\hat{\mathbf{g}}_{l'k}\|^2 \right\}, \quad (\text{B.4}) \end{aligned}$$

which represents the correlation between $\|\hat{\mathbf{g}}_{lk}\|^2$ and $\|\hat{\mathbf{g}}_{l'k}\|^2$, $l \neq l'$. Based on (3)–(8), (15), and (17), we can write

$$\begin{aligned} \hat{\mathbf{g}}_{lk} &= \boldsymbol{\mu}_{lk} + \sqrt{\tau_p \rho_p} \tilde{\mathbf{C}}_{lk} \mathbf{E}_{lk}^{-1} \\ &\quad \times \left(\sqrt{\tau_p \rho_p} \left(\tilde{\mathbf{h}}_{lk} + \sum_{k' \neq k} \tilde{\mathbf{h}}_{lk'} \boldsymbol{\varphi}_{k'}^H \boldsymbol{\varphi}_k \right) + \tilde{\mathbf{z}}_{lk} \right) \end{aligned}$$

with

$$\begin{aligned} \tilde{\mathbf{h}}_{lk} &\triangleq \sqrt{\beta_{lk}^{\text{UA}} \tilde{\mathbf{h}}_{lk}^{\text{UA}}} + \sum_{m=1}^M \sum_{n=1}^N \alpha_{mn} \left(\mu_{kmn}^{\text{US}} \sqrt{\beta_{lm}^{\text{SA}} \tilde{\mathbf{h}}_{lmn}^{\text{SA}}} \right. \\ &\quad \left. + \boldsymbol{\mu}_{lmn}^{\text{SA}} \sqrt{\beta_{km}^{\text{US}} \tilde{h}_{kmn}^{\text{US}}} + \sqrt{\beta_{lm}^{\text{SA}} \tilde{\mathbf{h}}_{lmn}^{\text{SA}}} \sqrt{\beta_{km}^{\text{US}} \tilde{h}_{kmn}^{\text{US}}} \right) \\ &= \sqrt{\beta_{lk}^{\text{UA}} \tilde{\mathbf{h}}_{lk}^{\text{UA}}} + \sum_{m=1}^M \sum_{n=1}^N \alpha_{mn} \mu_{kmn}^{\text{US}} \sqrt{\beta_{lm}^{\text{SA}} \tilde{\mathbf{h}}_{lmn}^{\text{SA}}} \\ &\quad + \sum_{m=1}^M \sum_{n=1}^N \alpha_{mn} \sqrt{\frac{\zeta_{lm}^{\text{SA}} \kappa_{lm}^{\text{SA}}}{\kappa_{lm}^{\text{SA}} + 1} \tilde{\mathbf{h}}_{lmn}^{\text{SA}}} \sqrt{\beta_{km}^{\text{US}} \tilde{h}_{kmn}^{\text{US}}} \\ &\quad + \sum_{m=1}^M \sum_{n=1}^N \alpha_{mn} \sqrt{\beta_{lm}^{\text{SA}} \tilde{\mathbf{h}}_{lmn}^{\text{SA}}} \sqrt{\beta_{km}^{\text{US}} \tilde{h}_{kmn}^{\text{US}}}, \quad (\text{B.5}) \end{aligned}$$

where the second equality follows the definition in (5). The correlation $r_{l'k}$ comes from the common channel coefficient $\tilde{h}_{kmn}^{\text{US}}$ in both $\hat{\mathbf{g}}_{lk}$ and $\hat{\mathbf{g}}_{l'k}$, $l \neq l'$, as observed in the last two terms in (B.5). However, these terms are very small compared to the overall channel coefficients of $\hat{\mathbf{g}}_{lk}$. This is because a HR-RIS is placed in the vicinity of either UEs or APs to improve

the system performance. The former case ensures strong LoS links between HR-RISs and UEs, but causes weak LoS links and large distances between APs and HR-RISs, leading to $\sqrt{\beta_{lm}^{\text{SA}} \tilde{\mathbf{h}}_{lmn}^{\text{SA}}} \approx \mathbf{0}$ and $\zeta_{lm}^{\text{SA}} \kappa_{lm}^{\text{SA}} \approx 0$. Under a similar analysis for the latter case, we have $\frac{\kappa_{lm}^{\text{SA}}}{\kappa_{lm}^{\text{SA}}+1} \approx 1$ and $\sqrt{\beta_{km}^{\text{US}} \tilde{h}_{kmn}^{\text{US}}} \approx 0$. Therefore, in both cases, the correlation between $\tilde{\mathbf{g}}_{lk}$ and $\hat{\mathbf{g}}_{l'k}$ are negligible, yielding $r_{l'k} \approx 0$. With this approximation, from (B.3), we obtain

$$\begin{aligned} \mathbb{E}\{|\text{BU}_{d,k}|^2\} &\approx \rho_d \sum_{l=1}^L \eta_{lk} \mathbb{E} \left\{ \left| \mathbf{g}_{lk}^T \hat{\mathbf{g}}_{lk}^* - \mathbb{E} \left\{ \mathbf{g}_{lk}^T \hat{\mathbf{g}}_{lk}^* \right\} \right|^2 \right\} \\ &= \rho_d \sum_{l=1}^L \eta_{lk} \left(\mathbb{E} \left\{ \left| \mathbf{g}_{lk}^T \hat{\mathbf{g}}_{lk}^* \right|^2 \right\} - \left| \mathbb{E} \left\{ \mathbf{g}_{lk}^T \hat{\mathbf{g}}_{lk}^* \right\} \right|^2 \right) \\ &= \rho_d \sum_{l=1}^L \eta_{lk} \left[\mathbb{E} \left\{ \|\hat{\mathbf{g}}_{lk}\|^4 \right\} + \mathbb{E} \left\{ \left| \tilde{\mathbf{g}}_{lk}^H \hat{\mathbf{g}}_{lk} \right|^2 \right\} \right. \\ &\quad \left. - \left(\text{trace}(\hat{\mathbf{C}}_{lk}) + \|\boldsymbol{\mu}_{lk}\|^2 \right)^2 \right], \quad (\text{B.6}) \end{aligned}$$

where the last term is based on the result in (B.1). Because the elements of $\tilde{\mathbf{g}}_{lk}$ and $\hat{\mathbf{g}}_{lk}$ are uncorrelated and $\mathbb{E}\{\tilde{\mathbf{g}}_{lk}\} = \mathbf{0}$, we have

$$\begin{aligned} \mathbb{E} \left\{ \left| \tilde{\mathbf{g}}_{lk}^H \hat{\mathbf{g}}_{lk} \right|^2 \right\} &= \mathbb{E} \left\{ \sum_{i=1}^{N_A} |\tilde{g}_{lki}^* \hat{g}_{lki}|^2 \right\} \\ &= \text{trace}(\tilde{\mathbf{R}}_{lk} \circ \hat{\mathbf{R}}_{lk}). \quad (\text{B.7}) \end{aligned}$$

To compute $\mathbb{E}\{\|\hat{\mathbf{g}}_{lk}\|^4\}$, we note that \mathbf{g}_{lk} is given in (8) as the sum of $MN+1$ vectors, where MN is the total number of elements of all the HR-RISs and is very large. Therefore, \mathbf{g}_{lk} and $\hat{\mathbf{g}}_{lk}$ can be approximated as $\mathbf{g}_{lk} \sim \mathcal{CN}(\boldsymbol{\mu}_{lk}, \mathbf{C}_{lk})$ and $\hat{\mathbf{g}}_{lk} \sim \mathcal{CN}(\boldsymbol{\mu}_{lk}, \hat{\mathbf{C}}_{lk})$, respectively. By [68, Lemma 9], it follows that

$$\begin{aligned} \mathbb{E} \left\{ \|\hat{\mathbf{g}}_{lk}\|^4 \right\} &= \|\boldsymbol{\mu}_{lk}\|^4 + 2 \|\boldsymbol{\mu}_{lk}\|^2 \text{trace}(\hat{\mathbf{C}}_{lk}) \\ &\quad + 2 \boldsymbol{\mu}_{lk}^H \hat{\mathbf{C}}_{lk} \boldsymbol{\mu}_{lk} + \left| \text{trace}(\hat{\mathbf{C}}_{lk}) \right|^2 + \text{trace}(\hat{\mathbf{C}}_{lk}^2). \quad (\text{B.8}) \end{aligned}$$

From (B.6), (B.7), and (B.8), we obtain

$$\begin{aligned} \mathbb{E}\{|\text{BU}_{d,k}|^2\} &\approx \rho_d \sum_{l=1}^L \eta_{lk} \underbrace{\left(2 \boldsymbol{\mu}_{lk}^H \hat{\mathbf{C}}_{lk} \boldsymbol{\mu}_{lk} + \text{trace}(\hat{\mathbf{C}}_{lk}^2 + \tilde{\mathbf{R}}_{lk} \circ \hat{\mathbf{R}}_{lk}) \right)}_{\triangleq d_{lk}(\boldsymbol{\alpha})}. \end{aligned}$$

By denoting $\mathbf{D}_{kk}(\boldsymbol{\alpha}) \triangleq \text{diag}\{d_{1kk}^{\frac{1}{2}}(\boldsymbol{\alpha}), \dots, d_{Lkk}^{\frac{1}{2}}(\boldsymbol{\alpha})\}$, $\mathbb{E}\{|\text{BU}_{d,k}|^2\}$ can be computed as

$$\mathbb{E}\{|\text{BU}_{d,k}|^2\} \approx \rho_d \|\mathbf{D}_{kk}(\{\alpha_{mn}\}) \bar{\boldsymbol{\eta}}_k\|^2. \quad (\text{B.9})$$

3) Compute $\mathbb{E}\{|\text{UI}_{d,kk'}|^2\}$: We rewrite $\hat{\mathbf{g}}_{lk'}$ in (A.12) as

$$\hat{\mathbf{g}}_{lk'} = \hat{\mathbf{g}}_{lk'} + \sqrt{\tau_p \rho_p} \mathbf{C}_{lk'} \mathbf{E}_{lk'}^{-1} \tilde{\mathbf{z}}_{lk'}, \quad (\text{B.10})$$

where

$$\hat{\mathbf{g}}_{lk'} \triangleq \boldsymbol{\mu}_{lk'} - \tau_p \rho_p \tilde{\mathbf{C}}_{lk'} \mathbf{E}_{lk'}^{-1} \tilde{\boldsymbol{\mu}}_{lk'} + \tau_p \rho_p \tilde{\mathbf{C}}_{lk'} \mathbf{E}_{lk'}^{-1} \sum_{k=1}^K \mathbf{g}_{lk} \boldsymbol{\varphi}_k^H \boldsymbol{\varphi}_{k'}.$$

As a result, $\mathbb{E} \left\{ |\text{UI}_{d,kk'}|^2 \right\}$ is computed as

$$\begin{aligned} \mathbb{E} \left\{ |\text{UI}_{d,kk'}|^2 \right\} &= \mathbb{E} \left\{ \left| \sqrt{\rho_d} \sum_{l=1}^L \sqrt{\eta_{lk'}} \mathbf{g}_{lk'}^T \hat{\mathbf{g}}_{lk'}^* \right|^2 \right\} \\ &= \rho_d \mathbb{E} \left\{ \left| \sum_{l=1}^L \sqrt{\eta_{lk'}} \mathbf{g}_{lk'}^T \hat{\mathbf{g}}_{lk'}^* + \sqrt{\eta_{lk'}} \sqrt{\tau_p \rho_p} \mathbf{g}_{lk'}^T \check{\mathbf{C}}_{lk'} \mathbf{E}_{lk'}^{-1} \check{\mathbf{z}}_{lk'}^* \right|^2 \right\} \\ &= \rho_d \mathbb{E} \left\{ \left| \sum_{l=1}^L \sqrt{\eta_{lk'}} \mathbf{g}_{lk'}^T \hat{\mathbf{g}}_{lk'}^* \right|^2 \right\} \\ &\quad + \rho_d \mathbb{E} \left\{ \left| \sum_{l=1}^L \sqrt{\eta_{lk'}} \sqrt{\tau_p \rho_p} \mathbf{g}_{lk'}^T \check{\mathbf{C}}_{lk'} \mathbf{E}_{lk'}^{-1} \check{\mathbf{z}}_{lk'}^* \right|^2 \right\} \\ &= \rho_d \text{Var} \left(\sum_{l=1}^L \sqrt{\eta_{lk'}} \mathbf{g}_{lk'}^T \hat{\mathbf{g}}_{lk'}^* \right) + \rho_d \left| \mathbb{E} \left\{ \sum_{l=1}^L \sqrt{\eta_{lk'}} \mathbf{g}_{lk'}^T \hat{\mathbf{g}}_{lk'}^* \right\} \right|^2 \\ &\quad + \rho_d \mathbb{E} \left\{ \left| \sum_{l=1}^L \sqrt{\eta_{lk'}} \sqrt{\tau_p \rho_p} \mathbf{g}_{lk'}^T \check{\mathbf{C}}_{lk'} \mathbf{E}_{lk'}^{-1} \check{\mathbf{z}}_{lk'}^* \right|^2 \right\}. \quad (\text{B.11}) \end{aligned}$$

Let us denote by \mathcal{T}_1 , \mathcal{T}_2 , and \mathcal{T}_3 the three terms in (B.11), from left to right, respectively. To compute these terms, we use $\mathbb{E} \{ \mathbf{g}_{lk} \} = \boldsymbol{\mu}_{lk}$, $\mathbb{E} \{ \hat{\mathbf{g}}_{lk'} \} = \boldsymbol{\mu}_{lk'}$, and

$$\begin{aligned} \mathbb{C} \{ \hat{\mathbf{g}}_{lk'} \} &= \tau_p^2 \rho_p^2 \check{\mathbf{C}}_{lk'} \mathbf{E}_{lk'}^{-1} \left(\sum_{\bar{k}=1}^K |\varphi_{\bar{k}}^H \varphi_{\bar{k}}|^2 \mathbf{C}_{l\bar{k}} \right) \mathbf{E}_{lk'}^{-H} \check{\mathbf{C}}_{lk'}^H \\ &\triangleq \hat{\mathbf{C}}_{lk'}, \end{aligned}$$

based on the definition of $\hat{\mathbf{g}}_{lk'}$. Furthermore, we note that in \mathcal{T}_1 and \mathcal{T}_2 , \mathbf{g}_{lk} and $\hat{\mathbf{g}}_{lk'}$ are correlated due to the second term in (B.5), which can be rewritten as

$$\begin{aligned} \sum_{m=1}^M \sum_{n=1}^N \alpha_{mn} \mu_{kmn}^{\text{US}} \sqrt{\beta_{lm}^{\text{SA}} \tilde{\mathbf{h}}_{lmn}^{\text{SA}}} \\ = \sum_{m=1}^M \sum_{n=1}^N \alpha_{mn} \sqrt{\frac{\zeta_{km}^{\text{US}} \kappa_{km}^{\text{US}}}{\kappa_{km}^{\text{UA}} + 1}} \tilde{h}_{kmn}^{\text{US}} \sqrt{\beta_{lm}^{\text{SA}} \tilde{\mathbf{h}}_{lmn}^{\text{SA}}}, \end{aligned}$$

based on (4). By a similar analysis in the previous subsection, we can show that this term is very small compared to the overall coefficients of \mathbf{g}_{lk} and $\hat{\mathbf{g}}_{lk'}$. Specifically, we have $\sqrt{\beta_{lm}^{\text{SA}} \tilde{\mathbf{h}}_{lmn}^{\text{SA}}} \approx \mathbf{0}$, $\frac{\kappa_{km}^{\text{US}}}{\kappa_{km}^{\text{UA}} + 1} \approx 1$ or $\zeta_{km}^{\text{US}} \kappa_{km}^{\text{US}} \approx 0$ when HR-RISs are deployed in the vicinity of either UEs or APs, respectively. Therefore, the correlation between \mathbf{g}_{lk} and $\hat{\mathbf{g}}_{lk'}$ can be neglected. A similar observation can be made for the correlation between \mathbf{g}_{lk} and $\check{\mathbf{z}}_{lk'}$ in \mathcal{T}_3 because of the common term $\sqrt{\beta_{lm}^{\text{SA}} \tilde{\mathbf{h}}_{lmn}^{\text{SA}}}$ (as seen in (4) and (16)). Therefore, \mathcal{T}_1 , \mathcal{T}_2 , and \mathcal{T}_3 can be approximated as

$$\begin{aligned} \mathcal{T}_1 &\approx \rho_d \sum_{l=1}^L \eta_{lk'} \sum_{t=1}^{N_A} \text{Var} (g_{lkt} \check{g}_{lk't}^*) = \rho_d \sum_{l=1}^L \eta_{lk'} \\ &\quad \times \text{trace} \left(\mathbf{C}_{lk} \circ \check{\mathbf{C}}_{lk'} + \mathbf{C}_{lk} \boldsymbol{\mu}_{lk'} \boldsymbol{\mu}_{lk'}^H + \check{\mathbf{C}}_{lk'} \boldsymbol{\mu}_{lk} \boldsymbol{\mu}_{lk}^H \right), \quad (\text{B.12}) \end{aligned}$$

$$\mathcal{T}_2 \approx \rho_d \left| \sum_{l=1}^L \sqrt{\eta_{lk'}} \boldsymbol{\mu}_{lk'}^T \boldsymbol{\mu}_{lk'}^* \right|^2 = \rho_d \left| \mathbf{v}_{kk'}^T(\boldsymbol{\alpha}) \bar{\boldsymbol{\eta}}_{k'} \right|^2, \quad (\text{B.13})$$

$$\begin{aligned} \mathcal{T}_3 &\approx \rho_d \sum_{l=1}^L \eta_{lk'} \tau_p \rho_p \mathbb{E} \left\{ \left| \mathbf{g}_{lk'}^T \check{\mathbf{C}}_{lk'} \mathbf{E}_{lk'}^{-1} \check{\mathbf{z}}_{lk'}^* \right|^2 \right\} \\ &= \rho_d \sum_{l=1}^L \eta_{lk'} \tau_p \rho_p \sigma_{p,l}^2 \text{trace} \left(\mathbf{R}_{lk} \check{\mathbf{C}}_{lk'} \mathbf{E}_{lk'}^{-1} (\check{\mathbf{C}}_{lk'} \mathbf{E}_{lk'}^{-1})^H \right). \quad (\text{B.14}) \end{aligned}$$

In (B.13), $\mathbf{v}_{kk'}(\boldsymbol{\alpha})$ is defined as $\mathbf{v}_{kk'}(\boldsymbol{\alpha}) \triangleq [v_{1kk'}(\boldsymbol{\alpha}), \dots, v_{Lkk'}(\boldsymbol{\alpha})]^T$ with $v_{lkk'}(\boldsymbol{\alpha}) \triangleq \boldsymbol{\mu}_{lk}^T \boldsymbol{\mu}_{lk'}^*$. From (B.12)–(B.14), we obtain $\mathbb{E} \left\{ |\text{UI}_{d,kk'}|^2 \right\}$ as $\mathcal{T}_1 + \mathcal{T}_2 + \mathcal{T}_3$. The expression can be shortened by the fact that $\text{trace}(\mathbf{A} + \mathbf{B}) = \text{trace}(\mathbf{A}) + \text{trace}(\mathbf{B})$. Specifically, by letting

$$\begin{aligned} \bar{\mathbf{C}}_{lkk'} &\triangleq \mathbf{C}_{lk} \circ \hat{\mathbf{C}}_{lk'} + \mathbf{C}_{lk} \boldsymbol{\mu}_{lk'} \boldsymbol{\mu}_{lk'}^H + \hat{\mathbf{C}}_{lk'} \boldsymbol{\mu}_{lk} \boldsymbol{\mu}_{lk}^H \\ &\quad + \tau_p \rho_p \sigma_{p,l}^2 \mathbf{R}_{lk} \check{\mathbf{C}}_{lk'} \mathbf{E}_{lk'}^{-1} (\check{\mathbf{C}}_{lk'} \mathbf{E}_{lk'}^{-1})^H, \quad (\text{B.15}) \end{aligned}$$

we can write $\mathbb{E} \left\{ |\text{UI}_{d,kk'}|^2 \right\}$ in a more compact form as

$$\begin{aligned} \mathbb{E} \left\{ |\text{UI}_{d,kk'}|^2 \right\} \\ &\approx \rho_d \left| \mathbf{v}_{kk'}^T(\boldsymbol{\alpha}) \bar{\boldsymbol{\eta}}_{k'} \right|^2 + \rho_d \sum_{l=1}^L \eta_{lk'} \text{trace}(\bar{\mathbf{C}}_{lkk'}) \\ &= \rho_d \left| \mathbf{v}_{kk'}^T(\boldsymbol{\alpha}) \bar{\boldsymbol{\eta}}_{k'} \right|^2 + \rho_d \|\mathbf{D}_{kk'}(\boldsymbol{\alpha}) \bar{\boldsymbol{\eta}}_{k'}\|^2, \quad (\text{B.16}) \end{aligned}$$

where $\mathbf{D}_{kk'}(\boldsymbol{\alpha}) \triangleq \text{diag} \left\{ d_{1kk'}^{\frac{1}{2}}(\boldsymbol{\alpha}), \dots, d_{Lkk'}^{\frac{1}{2}}(\boldsymbol{\alpha}) \right\}$, with

$$\begin{aligned} d_{lkk'}(\boldsymbol{\alpha}) &\triangleq \text{trace}(\bar{\mathbf{C}}_{lkk'}) \\ &= \boldsymbol{\mu}_{lk'}^H \mathbf{C}_{lk} \boldsymbol{\mu}_{lk'} + \boldsymbol{\mu}_{lk}^H \hat{\mathbf{C}}_{lk'} \boldsymbol{\mu}_{lk} + \text{trace}(\mathbf{T}_{lkk'}). \end{aligned}$$

Here, $\mathbf{T}_{lkk'} \triangleq \mathbf{C}_{lk} \circ \hat{\mathbf{C}}_{lk'} + \tau_p \rho_p \sigma_{p,l}^2 \mathbf{R}_{lk} \check{\mathbf{C}}_{lk'} \mathbf{E}_{lk'}^{-1} (\check{\mathbf{C}}_{lk'} \mathbf{E}_{lk'}^{-1})^H$. The results in (B.9) and (B.16) yields

$$\begin{aligned} \mathbb{E} \left\{ |\text{BU}_{d,k}|^2 \right\} + \sum_{k' \neq k}^K \mathbb{E} \left\{ |\text{UI}_{d,kk'}|^2 \right\} \\ \approx \rho_d \sum_{k' \neq k}^K \left| \mathbf{v}_{kk'}^T(\boldsymbol{\alpha}) \bar{\boldsymbol{\eta}}_{k'} \right|^2 + \rho_d \sum_{k'=1}^K \|\mathbf{D}_{kk'}(\boldsymbol{\alpha}) \bar{\boldsymbol{\eta}}_{k'}\|^2. \quad (\text{B.17}) \end{aligned}$$

By substituting the results in (B.2) and (B.17) into (30), we obtain (31), which completes the proof.

APPENDIX C PROOF OF THEOREM 3

Similar to the proof of Theorem 2, we compute $|\text{DS}_{u,k}|^2$, $\mathbb{E} \left\{ |\text{BU}_{u,k}|^2 \right\}$, $\mathbb{E} \left\{ |\text{UI}_{u,kk'}|^2 \right\}$, and $\mathbb{E} \left\{ |\tilde{z}_{u,k}|^2 \right\}$ to show the closed-form of $\text{SE}_{u,k}$ in (48). First, leveraging the derivation in (B.1), we obtain

$$\text{DS}_{u,k} = \sqrt{\rho_u \vartheta_k} \sum_{l=1}^L \omega_{lk} \mathbb{E} \left\{ \mathbf{g}_{lk}^H \hat{\mathbf{g}}_{lk} \right\} = \sqrt{\rho_u \vartheta_k} \sum_{l=1}^L \omega_{lk} u_{lk}(\boldsymbol{\alpha}),$$

and thus,

$$|\text{DS}_{u,k}|^2 = \rho_u \vartheta_k \left| \sum_{l=1}^L \omega_{lk} u_{lk}(\boldsymbol{\alpha}) \right|^2 = \rho_u \vartheta_k \left| \mathbf{u}_k(\boldsymbol{\alpha})^T \boldsymbol{\omega}_k \right|^2, \quad (\text{C.1})$$

where $\boldsymbol{\omega}_k \triangleq [\omega_{1k}, \dots, \omega_{Lk}]^T$. To derive $\mathbb{E}\left\{|\text{BU}_{u,k}|^2\right\}$, we rewrite

$$\text{BU}_{u,k} = \sqrt{\rho_u \vartheta_k} \sum_{l=1}^L \omega_{lk} \left(\mathbf{g}_{lk}^H \hat{\mathbf{g}}_{lk} - \mathbb{E}\left\{ \mathbf{g}_{lk}^H \hat{\mathbf{g}}_{lk} \right\} \right),$$

and similar to (B.6), we obtain

$$\begin{aligned} & \mathbb{E}\left\{|\text{BU}_{u,k}|^2\right\} \\ & \approx \rho_u \vartheta_k \sum_{l=1}^L \mathbb{E}\left\{ \left| \omega_{lk} \left(\mathbf{g}_{lk}^H \hat{\mathbf{g}}_{lk} - \mathbb{E}\left\{ \mathbf{g}_{lk}^H \hat{\mathbf{g}}_{lk} \right\} \right) \right|^2 \right\} \\ & = \rho_u \vartheta_k \sum_{l=1}^L \omega_{lk}^2 \left(\mathbb{E}\left\{ \|\hat{\mathbf{g}}_{lk}\|^4 \right\} + \mathbb{E}\left\{ \left| \tilde{\mathbf{g}}_{lk}^H \hat{\mathbf{g}}_{lk} \right|^2 \right\} \right. \\ & \quad \left. - \left(\text{trace}\left(\hat{\mathbf{C}}_{lk}\right) + \|\boldsymbol{\mu}_{lk}\|^2 \right)^2 \right) \\ & = \rho_u \vartheta_k \sum_{l=1}^L \omega_{lk}^2 d_{lkk}(\boldsymbol{\alpha}) = \rho_u \vartheta_k \|\mathbf{D}_{kk}(\boldsymbol{\alpha})\boldsymbol{\omega}_k\|^2. \quad (\text{C.2}) \end{aligned}$$

Similar to (B.11), we express $\mathbb{E}\left\{|\text{UI}_{u,kk'}|^2\right\}$ as

$$\begin{aligned} & \mathbb{E}\left\{|\text{UI}_{u,kk'}|^2\right\} = \sqrt{\rho_u \vartheta_{k'}} \mathbb{V}\text{ar}\left(\sum_{l=1}^L \omega_{lk'} \mathbf{g}_{lk'}^H \hat{\mathbf{g}}_{lk'} \right) \\ & + \sqrt{\rho_u \vartheta_{k'}} \left| \mathbb{E}\left\{ \sum_{l=1}^L \omega_{lk'} \mathbf{g}_{lk'}^H \hat{\mathbf{g}}_{lk'} \right\} \right|^2 \\ & + \sqrt{\rho_u \vartheta_{k'}} \mathbb{E}\left\{ \sum_{l=1}^L \left| \sqrt{\tau_p \rho_p} \omega_{lk'} \mathbf{g}_{lk'}^H \check{\mathbf{C}}_{lk'} \mathbf{E}_{lk'}^{-1} \tilde{\mathbf{z}}_{lk'} \right|^2 \right\}. \quad (\text{C.3}) \end{aligned}$$

Let us denote by \mathcal{J}_1 , \mathcal{J}_2 , and \mathcal{J}_3 the three terms in (C.3), from left to right, respectively. Similar to Appendix B, \mathcal{J}_1 , \mathcal{J}_2 , and \mathcal{J}_3 are computed as

$$\begin{aligned} \mathcal{J}_1 & \approx \rho_u \vartheta_{k'} \sum_{l=1}^L |\omega_{lk'}|^2 \sum_{t=1}^{N_A} \mathbb{V}\text{ar}\left(g_{lkt} \check{g}_{lkt}^* \right) = \rho_u \vartheta_{k'} \sum_{l=1}^L |\omega_{lk'}|^2 \\ & \quad \times \text{trace}\left(\mathbf{C}_{lk} \circ \check{\mathbf{C}}_{lk'} + \mathbf{C}_{lk} \boldsymbol{\mu}_{lk'} \boldsymbol{\mu}_{lk'}^H + \check{\mathbf{C}}_{lk'} \boldsymbol{\mu}_{lk} \boldsymbol{\mu}_{lk}^H \right), \\ \mathcal{J}_2 & \approx \rho_u \vartheta_{k'} \left| \sum_{l=1}^L \omega_{lk'} \boldsymbol{\mu}_{lk'}^H \boldsymbol{\mu}_{lk'} \right|^2 \\ & = \rho_u \vartheta_{k'} \left| \sum_{l=1}^L \omega_{lk'} v_{lk'}(\boldsymbol{\alpha}) \right|^2 = \rho_u \vartheta_{k'} \left| \mathbf{v}_{kk'}^T(\boldsymbol{\alpha}) \boldsymbol{\omega}_{k'} \right|^2, \\ \mathcal{J}_3 & \approx \rho_u \vartheta_{k'} \sum_{l=1}^L \tau_p \rho_p \mathbb{E}\left\{ \left| \omega_{lk'} \mathbf{g}_{lk'}^H \check{\mathbf{C}}_{lk'} \mathbf{E}_{lk'}^{-1} \tilde{\mathbf{z}}_{lk'} \right|^2 \right\} \\ & = \rho_u \vartheta_{k'} \sum_{l=1}^L |\omega_{lk'}|^2 \tau_p \rho_p \sigma_{p,l}^2 \\ & \quad \times \text{trace}\left(\left(\check{\mathbf{C}}_{lk'} + \boldsymbol{\mu}_{lk} \boldsymbol{\mu}_{lk}^H \right) \mathbf{C}_{lk'} \mathbf{E}_{lk'}^{-1} \left(\check{\mathbf{C}}_{lk'} \mathbf{E}_{lk'}^{-1} \right)^H \right). \end{aligned}$$

As a result, $\mathbb{E}\left\{|\text{UI}_{u,kk'}|^2\right\}$ can be written in the following compact form

$$\begin{aligned} & \mathbb{E}\left\{|\text{UI}_{u,kk'}|^2\right\} \\ & \approx \rho_u \vartheta_{k'} \left| \mathbf{v}_{kk'}^T(\boldsymbol{\alpha}) \boldsymbol{\omega}_{k'} \right|^2 + \rho_u \vartheta_{k'} \|\mathbf{D}_{kk'}(\boldsymbol{\alpha})\boldsymbol{\omega}_{k'}\|^2. \quad (\text{C.4}) \end{aligned}$$

The results in (C.2) and (C.4) yields

$$\begin{aligned} & \mathbb{E}\left\{|\text{BU}_{u,k}|^2\right\} + \sum_{k' \neq k}^K \mathbb{E}\left\{|\text{UI}_{u,kk'}|^2\right\} \\ & \approx \rho_u \sum_{k' \neq k}^K \vartheta_{k'} \left| \mathbf{v}_{kk'}^T(\boldsymbol{\alpha}) \boldsymbol{\omega}_{k'} \right|^2 \\ & \quad + \rho_u \sum_{k'=1}^K \vartheta_{k'} \|\mathbf{D}_{kk'}(\boldsymbol{\alpha})\boldsymbol{\omega}_{k'}\|^2. \quad (\text{C.5}) \end{aligned}$$

To complete the proof, we compute the term $\mathbb{E}\left\{|\tilde{z}_{u,k}|^2\right\}$ in (47) as follows:

$$\begin{aligned} & \mathbb{E}\left\{|\tilde{z}_{u,k}|^2\right\} = \sum_{l=1}^L \mathbb{E}\left\{ \left| \omega_{lk} \hat{\mathbf{g}}_{lk}^H \mathbf{z}_{u,l} \right|^2 \right\} \\ & \approx \sum_{l=1}^L \omega_{lk}^2 \sigma_{u,l}^2 \left(\text{trace}\left(\hat{\mathbf{C}}_{lk}\right) + \|\boldsymbol{\mu}_{lk}\|^2 \right), \end{aligned}$$

where the approximation is made because the correlation between $\mathbf{z}_{u,l}$ and $\hat{\mathbf{g}}_{lk}$ is negligible, based on a similar observation as in Appendix B. Furthermore, by recalling that $u_{lk}(\boldsymbol{\alpha}) = \text{trace}\left(\hat{\mathbf{C}}_{lk}\right) + \|\boldsymbol{\mu}_{lk}\|^2$ and denoting $\boldsymbol{\Sigma}_k(\boldsymbol{\alpha}) \triangleq \text{diag}\left\{ \sigma_{u,1} \sqrt{u_{1k}(\boldsymbol{\alpha})}, \dots, \sigma_{u,L} \sqrt{u_{Lk}(\boldsymbol{\alpha})} \right\}$, we obtain

$$\mathbb{E}\left\{|\tilde{z}_{u,k}|^2\right\} = \sum_{l=1}^L \omega_{lk}^2 \sigma_{u,l}^2 u_{lk}(\boldsymbol{\alpha}) = \|\boldsymbol{\Sigma}_k(\boldsymbol{\alpha})\boldsymbol{\omega}_k\|^2. \quad (\text{C.6})$$

Finally, by substituting the results in (C.1), (C.5), and (C.6) into (47), we obtain (48).

REFERENCES

- [1] H. Q. Ngo, A. Ashikhmin, H. Yang, E. G. Larsson, and T. L. Marzetta, "Cell-free massive MIMO versus small cells," *IEEE Trans. Wireless Commun.*, vol. 16, no. 3, pp. 1834–1850, 2017.
- [2] H. Q. Ngo, L.-N. Tran, T. Q. Duong, M. Matthaiou, and E. G. Larsson, "On the total energy efficiency of cell-free massive MIMO," *IEEE Trans. Green Commun. Network.*, vol. 2, no. 1, pp. 25–39, 2017.
- [3] Q. Wu and R. Zhang, "Towards smart and reconfigurable environment: Intelligent reflecting surface aided wireless network," *IEEE Commun. Mag.*, vol. 58, no. 1, pp. 106–112, Nov. 2019.
- [4] P. Xu, G. Chen, Z. Yang, and M. Di Renzo, "Reconfigurable intelligent surfaces assisted communications with discrete phase shifts: How many quantization levels are required to achieve full diversity?" *IEEE Wireless Commun. Lett.*, vol. 10, no. 2, pp. 358–362, 2020.
- [5] M. Di Renzo, K. Ntontin, J. Song, F. H. Danufane, X. Qian, F. Lazarakis, J. De Rosny, D.-T. Phan-Huy, O. Simeone, R. Zhang *et al.*, "Reconfigurable intelligent surfaces vs. relaying: Differences, similarities, and performance comparison," *IEEE IEEE Open J. Commun. Society*, vol. 1, pp. 798–807, 2020.
- [6] N. T. Nguyen, Q.-D. Vu, K. Lee, and M. Juntti, "Spectral efficiency optimization for hybrid relay-reflecting intelligent surface," in *Proc. IEEE Int. Conf. Commun. Workshop*, 2021, pp. 1–6.
- [7] —, "Hybrid relay-reflecting intelligent surface-assisted wireless communications," *IEEE Trans. Veh. Technol.*, vol. 71, no. 6, pp. 6228–6244, 2022.
- [8] N. T. Nguyen *et al.*, "Hybrid relay-reflecting intelligent surface-aided wireless communications: Opportunities, challenges, and future perspectives," *arXiv*, 2021. [Online]. Available: <https://arxiv.org/abs/2104.02039>
- [9] Q. Wu and R. Zhang, "Beamforming optimization for wireless network aided by intelligent reflecting surface with discrete phase shifts," *IEEE Trans. Commun.*, vol. 68, no. 3, pp. 1838–1851, 2019.
- [10] E. Basar, M. Di Renzo, J. De Rosny, M. Debbah, M. Alouini, and R. Zhang, "Wireless communications through reconfigurable intelligent surfaces," *IEEE Access*, vol. 7, pp. 116 753–116 773, 2019.
- [11] C. Huang, A. Zappone, G. C. Alexandropoulos, M. Debbah, and C. Yuen, "Reconfigurable intelligent surfaces for energy efficiency in wireless communication," *IEEE Trans. Wireless Commun.*, vol. 18, no. 8, pp. 4157–4170, 2019.
- [12] J. He, H. Wymeersch, L. Kong, O. Silvén, and M. Juntti, "Large intelligent surface for positioning in millimeter wave MIMO systems," in *Proc. IEEE Veh. Technol. Conf.*, 2020, pp. 1–5.
- [13] N. T. Nguyen, L. V. Nguyen, T. Huynh-The, D. H. Nguyen, A. L. Swindlehurst, and M. Juntti, "Machine learning-based reconfigurable intelligent surface-aided MIMO systems," in *Proc. IEEE Works. on Sign. Proc. Adv. in Wirel. Comms.*, 2021, pp. 101–105.
- [14] A. Shojaeifard, K.-K. Wong, K.-F. Tong, Z. Chu, A. Mourad, A. Haghghat, I. Hemadeh, N. T. Nguyen, V. Tapio, and M. Juntti, "MIMO evolution beyond 5G through reconfigurable intelligent surfaces and fluid antenna systems," *Proceedings of the IEEE*, vol. 110, no. 9, pp. 1244–1265, 2022.

- [15] Y. Yang, B. Zheng, S. Zhang, and R. Zhang, "Intelligent reflecting surface meets OFDM: Protocol design and rate maximization," *IEEE Trans. Commun.*, vol. 68, no. 7, pp. 4522–4535, 2020.
- [16] Q. Wu and R. Zhang, "Intelligent reflecting surface enhanced wireless network via joint active and passive beamforming," *IEEE Trans. Wireless Commun.*, vol. 18, no. 11, pp. 5394–5409, 2019.
- [17] P. Wang, J. Fang, X. Yuan, Z. Chen, and H. Li, "Intelligent reflecting surface-assisted millimeter wave communications: Joint active and passive precoding design," *IEEE Trans. Veh. Technol.*, vol. 69, no. 12, pp. 14960–14973, 2020.
- [18] X. Yu, D. Xu, and R. Schober, "MISO wireless communication systems via intelligent reflecting surfaces," in *Proc. IEEE Int. Conf. Commun.*, 2019, pp. 735–740.
- [19] Y. Yang, S. Zhang, and R. Zhang, "IRS-enhanced OFDM: Power allocation and passive array optimization," in *Proc. IEEE Global Commun. Conf.*, 2019, pp. 1–6.
- [20] J. Yuan, Y.-C. Liang, J. Joung, G. Feng, and E. G. Larsson, "Intelligent reflecting surface-assisted cognitive radio system," *IEEE Trans. Commun.*, vol. 69, no. 1, pp. 675–687, 2020.
- [21] Y. Han, W. Tang, S. Jin, C.-K. Wen, and X. Ma, "Large intelligent surface-assisted wireless communication exploiting statistical CSI," *IEEE Trans. Veh. Technol.*, vol. 68, no. 8, pp. 8238–8242, 2019.
- [22] B. Di, H. Zhang, L. Li, L. Song, Y. Li, and Z. Han, "Practical hybrid beamforming with finite-resolution phase shifters for reconfigurable intelligent surface based multi-user communications," *IEEE Trans. Veh. Technol.*, vol. 69, no. 4, pp. 4565–4570, 2020.
- [23] S. Zhang and R. Zhang, "Capacity characterization for intelligent reflecting surface aided MIMO communication," *IEEE J. Sel. Areas Commun.*, vol. 38, no. 8, pp. 1823–1838, 2020.
- [24] K. Ying, Z. Gao, S. Lyu, Y. Wu, H. Wang, and M.-S. Alouini, "GMD-based hybrid beamforming for large reconfigurable intelligent surface assisted millimeter-wave massive MIMO," *IEEE Access*, vol. 8, pp. 19 530–19 539, 2020.
- [25] Y. Zhang, C. Zhong, Z. Zhang, and W. Lu, "Sum rate optimization for two way communications with intelligent reflecting surface," *IEEE Commun. Lett.*, vol. 24, no. 5, pp. 1090–1094, 2020.
- [26] N. S. Perović, L.-N. Tran, M. Di Renzo, and M. F. Flanagan, "Achievable rate optimization for MIMO systems with reconfigurable intelligent surfaces," *IEEE Trans. Wireless Commun.*, vol. 20, no. 6, pp. 3865–3882, 2021.
- [27] J. Xiong, L. You, Y. Huang, D. W. K. Ng, W. Wang, and X. Gao, "Reconfigurable intelligent surfaces assisted MIMO-MAC with partial CSI," in *Proc. IEEE Int. Conf. Commun.*, 2020, pp. 1–6.
- [28] Ö. Özdogan, E. Björnson, and E. G. Larsson, "Using intelligent reflecting surfaces for rank improvement in MIMO communications," in *Proc. IEEE Int. Conf. Acoust., Speech, Signal Processing*, 2020, pp. 9160–9164.
- [29] J. He, M. Leinonen, H. Wymeersch, and M. Juntti, "Channel estimation for RIS-aided mmWave MIMO systems," in *Proc. IEEE Global Commun. Conf.*, 2020, pp. 1–6.
- [30] J. He, N. T. Nguyen, R. Schroeder, V. Tapio, J. Kokkonen, and M. Juntti, "Channel estimation and hybrid architectures for RIS-assisted communications," *Joint EuCNC & 6G Summit*, 2021.
- [31] L. You *et al.*, "Reconfigurable intelligent surfaces-assisted multiuser MIMO uplink transmission with partial CSI," *IEEE Trans. Wireless Commun.*, vol. 20, no. 9, pp. 5613–5627, 2021.
- [32] C. Hu, L. Dai, S. Han, and X. Wang, "Two-timescale channel estimation for reconfigurable intelligent surface aided wireless communications," *IEEE Trans. Commun.*, vol. 69, no. 11, pp. 7736–7747, 2021.
- [33] G. C. Alexandropoulos and E. Vlachos, "A hardware architecture for reconfigurable intelligent surfaces with minimal active elements for explicit channel estimation," in *Proc. IEEE Int. Conf. Acoust., Speech, Signal Processing*, 2020, pp. 9175–9179.
- [34] J. He, H. Wymeersch, and M. Juntti, "Channel estimation for RIS-aided mmWave MIMO systems via atomic norm minimization," *IEEE Trans. Wireless Commun.*, vol. 20, no. 9, pp. 5786–5797, 2021.
- [35] H. Zhang, B. Di, L. Song, and Z. Han, "Reconfigurable intelligent surfaces assisted communications with limited phase shifts: How many phase shifts are enough?" *IEEE Trans. Veh. Technol.*, vol. 69, no. 4, pp. 4498–4502, 2020.
- [36] H. Guo, Y.-C. Liang, J. Chen, and E. G. Larsson, "Weighted Sum-Rate Maximization for Intelligent Reflecting Surface Enhanced Wireless Networks," in *Proc. IEEE Global Commun. Conf.*, 2019, pp. 1–6.
- [37] J. V. Alegria and F. Rusek, "Achievable rate with correlated hardware impairments in large intelligent surfaces," in *IEEE Int. Workshop Computational Advances in Multi-Sensor Adaptive Process. (CAMSAP)*, 2019, pp. 559–563.
- [38] Y. Zhang, B. Di, H. Zhang, J. Lin, Y. Li, and L. Song, "Reconfigurable intelligent surface aided cell-free MIMO communications," *IEEE Wireless Commun. Lett.*, vol. 10, no. 4, pp. 775–779, 2020.
- [39] Y. Zhang *et al.*, "Beyond cell-free MIMO: Energy efficient reconfigurable intelligent surface aided cell-free MIMO communications," *IEEE Trans. Cognitive Commun. Network.*, vol. 7, no. 2, pp. 412–426, 2021.
- [40] S. Huang, Y. Ye, M. Xiao, H. V. Poor, and M. Skoglund, "Decentralized beamforming design for intelligent reflecting surface-enhanced cell-free networks," *IEEE Wireless Commun. Lett.*, vol. 10, no. 3, pp. 673–677, 2020.
- [41] T. Van Chien, H. Q. Ngo, S. Chatzinotas, M. Di Renzo, and B. Ottersten, "Reconfigurable intelligent surface-assisted cell-free massive MIMO systems over spatially-correlated channels," *IEEE Trans. Wireless Commun.*, 2021.
- [42] T. Zhou, K. Xu, X. Xia, W. Xie, and X. Yang, "Achievable rate maximization for aerial intelligent reflecting surface-aided cell-free massive MIMO system," in *IEEE 6th Int. Conf. Computer Commun. (ICCC)*, 2020, pp. 623–628.
- [43] E. Björnson, O. Özdogan, and E. G. Larsson, "Intelligent reflecting surface vs. decode-and-forward: How large surfaces are needed to beat relaying?" *IEEE Wireless Commun. Lett.*, vol. 9, no. 2, pp. 244–248, 2019.
- [44] N. T. Nguyen, V.-D. Nguyen, Q. Wu, A. Tolli, S. Chatzinotas, and M. Juntti, "Hybrid active-passive reconfigurable intelligent surface-assisted multi-user MISO systems," in *Proc. IEEE Works. on Sign. Proc. Adv. in Wirel. Comms.*, 2022.
- [45] K.-H. Ngo *et al.*, "Low-latency and secure computation offloading assisted by hybrid relay-reflecting intelligent surface," in *IEEE Int. Conf. Advanced Technol. Commun. (ATC)*, 2021, pp. 306–311.
- [46] R. Long, Y.-C. Liang, Y. Pei, and E. G. Larsson, "Active reconfigurable intelligent surface aided wireless communications," *IEEE Trans. Wireless Commun.*, vol. 20, no. 8, pp. 4962–4975, 2021.
- [47] Z. Zhang, L. Dai, X. Chen, C. Liu, F. Yang, R. Schober, and H. V. Poor, "Active RIS vs. passive RIS: Which will prevail in 6G?" *arXiv preprint arXiv:2103.15154*, 2021.
- [48] M. H. Khoshafa, T. M. Ngatched, M. H. Ahmed, and A. R. Ndjiongue, "Active reconfigurable intelligent surfaces-aided wireless communication system," *IEEE Commun. Lett.*, vol. 25, no. 11, pp. 3699–3703, 2021.
- [49] C. You and R. Zhang, "Wireless communication aided by intelligent reflecting surface: Active or passive?" *IEEE Wireless Commun. Lett.*, vol. 10, no. 12, pp. 2659–2663, 2021.
- [50] K. Liu, Z. Zhang, L. Dai, S. Xu, and F. Yang, "Active reconfigurable intelligent surface: Fully-connected or sub-connected?" *IEEE Commun. Lett.*, vol. 26, no. 1, pp. 167–171, 2021.
- [51] N. Landsberg and E. Socher, "A low-power 28-nm CMOS FD-SOI reflection amplifier for an active F-band reflectarray," *IEEE Trans. Microw. Theory Techn.*, vol. 65, no. 10, pp. 3910–3921, May 2017.
- [52] A. Taha, M. Alrabeiah, and A. Alkhatib, "Deep learning for large intelligent surfaces in millimeter wave and massive MIMO systems," in *Proc. IEEE Global Commun. Conf.*, 2019, pp. 1–6.
- [53] W. Tang, X. Chen, M. Z. Chen, J. Y. Dai, Y. Han, S. Jin, Q. Cheng, G. Y. Li, and T. J. Cui, "On channel reciprocity in reconfigurable intelligent surface assisted wireless networks," *IEEE Wireless Commun.*, vol. 28, no. 6, pp. 94–101, 2021.
- [54] S. Atapattu *et al.*, "Reconfigurable intelligent surface assisted two-way communications: Performance analysis and optimization," *IEEE Trans. Commun.*, vol. 68, no. 10, pp. 6552–6567, 2020.
- [55] Ö. Özdogan, E. Björnson, and J. Zhang, "Cell-free massive MIMO with Rician fading: Estimation schemes and spectral efficiency," in *Proc. Annual Asilomar Conf. Signals, Syst., Comp.*, 2018, pp. 975–979.
- [56] Ö. Özdogan, E. Björnson, and J. Zhang, "Performance of cell-free massive MIMO with Rician fading and phase shifts," *IEEE Trans. Wireless Commun.*, vol. 18, no. 11, pp. 5299–5315, 2019.
- [57] Z. Wang, J. Zhang, E. Björnson, and B. Ai, "Uplink performance of cell-free massive MIMO over spatially correlated rician fading channels," *IEEE Commun. Lett.*, vol. 25, no. 4, pp. 1348–1352, 2020.
- [58] R. Malik and M. Vu, "Optimal transmission using a self-sustained relay in a full-duplex MIMO system," *IEEE J. Sel. Areas Commun.*, vol. 37, no. 2, pp. 374–390, 2018.
- [59] D. Bharadia and S. Katti, "Full duplex MIMO radios," in *11th USENIX Symp. Netw. Syst. Design Implement. (NSDI)*, 2014, pp. 359–372.
- [60] Q. Wu, S. Zhang, B. Zheng, C. You, and R. Zhang, "Intelligent reflecting surface aided wireless communications: A tutorial," *IEEE Trans. Commun.*, vol. 69, no. 5, pp. 3313–3351, Jan. 2021.

- [61] J. Zheng, J. Zhang, E. Björnson, and B. Ai, "Impact of channel aging on cell-free massive MIMO over spatially correlated channels," *IEEE Trans. Wireless Commun.*, vol. 20, no. 10, pp. 6451–6466, 2021.
- [62] M. Bashar *et al.*, "Uplink spectral and energy efficiency of cell-free massive MIMO with optimal uniform quantization," *IEEE Trans. Commun.*, vol. 69, no. 1, pp. 223–245, 2020.
- [63] E. Björnson and L. Sanguinetti, "Making cell-free massive MIMO competitive with MMSE processing and centralized implementation," *IEEE Trans. Wireless Commun.*, vol. 19, no. 1, pp. 77–90, 2019.
- [64] A. H. Jafari, D. López-Pérez, M. Ding, and J. Zhang, "Study on scheduling techniques for ultra dense small cell networks," in *Proc. IEEE Veh. Technol. Conf.*, 2015, pp. 1–6.
- [65] I. Rodriguez *et al.*, "Path loss validation for urban micro cell scenarios at 3.5 GHz compared to 1.9 GHz," in *Proc. IEEE Global Commun. Conf.*, 2013, pp. 3942–3947.
- [66] S.-N. Jin, D.-W. Yue, and H. H. Nguyen, "Spectral and energy efficiency in cell-free massive MIMO systems over correlated Rician fading," *IEEE Systems J.*, vol. 15, no. 2, pp. 2822–2833, 2020.
- [67] Z. Wang, J. Zhang, B. Ai, C. Yuen, and M. Debbah, "Uplink performance of cell-free massive MIMO with multi-antenna users over jointly-correlated Rayleigh fading channels," *IEEE Trans. Wireless Commun.*, vol. 21, no. 9, pp. 7391–7406, 2022.
- [68] T. Van Chien and H. Q. Ngo, "Massive MIMO channels," *Antennas and Propagation for 5G and Beyond*, pp. 301–333, 2020.